**Title:** Dopaminergic control of postnatal mammalian spinal network function is predominantly inhibitory

**Abbreviated title:** Dopaminergic control of dedicated spinal network components

**Authors:** Simon A. Sharples[1,2], Nicole E. Burma[1,2], Joanna Borowska-Fielding[3], Charlie H.T. Kwok[1,4], Shane E.A. Eaton[1,4], Glen B. Baker[5], Celine Jean-Xavier[4], Ying Zhang[3], Tuan Trang[1,4], Patrick J. Whelan[1,4]

**Affiliations :** [1] Hotchkiss Brain Institute, University of Calgary, Calgary, AB, Canada, T2N4N1, [2] Department of Neuroscience, University of Calgary, Calgary, AB, Canada, T2N 4N1, [3] Department of Medical Neuroscience, Dalhousie University, Halifax, NS, Canada, B3H 4R2.[4] Department of Comparative Biology and Experimental Medicine, University of Calgary, Calgary, AB, Canada, T2N4N1, [5] Department of Psychiatry (NRU), Faculty of Medicine and Dentistry, University of Alberta, Edmonton, AB, Canada. T6G 2G3.

**Correspondence:**
Dr. Patrick Whelan
HMRB 168
3330 Hospital Drive NW
Calgary, Alberta, Canada, T2N 4N1
whelan@ucalgary.ca

**Number of pages (text body)**: 27
**Number of Figures**: 9
**Number of Tables**: 2
**Word Count**: Abstract, (268) Introduction (579), Discussion (1555)

**Acknowledgments:** We would like to acknowledge support from the Whelan Lab and technical support from Dr. Heather Leduc-Pessah and Rebecca Dalgarno on immunoprecipitation experiments and from Gail Rauw on HPLC experiments. Spinalcore software was a kind gift from Prof A. Lev-Tov (Hebrew University).

**Funding:** We acknowledge studentships from the Natural Sciences and Engineering Research Council of Canada (SAS: NSERC-PGS-D), the Canadian Institute for Health Research (NEB, YZ), Alberta Innovates - Health Solutions (AIHS: SAS, NEB), Hotchkiss Brain Institute (SAS, NEB) and the Faculty of Veterinary Medicine (CHTK). This research was supported by grants to PJW provided by the Canadian Institutes of Health Research and NSERC (Discovery grant).

**Contributions:** SAS performed and analyzed whole-cell and network electrophysiology, NEB, performed and analyzed CoIP, GBB performed and analyzed HPLC, JBF performed recordings from V3 interneurons and SAS, CHTK and SEAE performed IHC and imaging experiments. SAS, CJ-X and PJW interpreted results. SAS prepared figures and drafted the manuscript. TT, YZ and PJW contributed to experimental design and procured funding. SAS, CJ-X and PJW conceived and designed the research. All authors reviewed and approved the final version of the manuscript.

**Abstract**

Dopamine is well known to regulate movement through the differential control of direct and indirect pathways in the striatum that express $D_1$ and $D_2$ receptors respectively. The spinal cord also expresses all dopamine receptors however; how the specific receptors regulate spinal network output in mammals is poorly understood. We explore the receptor-specific mechanisms that underlie dopaminergic control of spinal network output of neonatal mice during changes in spinal network excitability. During spontaneous activity, which is a characteristic of developing spinal networks operating in a low excitability state, we found that dopamine is primarily inhibitory. We uncover an excitatory $D_1$-mediated effect of dopamine on motoneurons and network output that also involves co-activation with $D_2$ receptors. Critically, these excitatory actions require higher concentrations of dopamine; however, analysis of dopamine concentrations of neonates indicates that endogenous levels of spinal dopamine are low. Because endogenous levels of spinal dopamine are low, this excitatory dopaminergic pathway is likely physiologically-silent at this stage in development. In contrast, the inhibitory effect of dopamine, at low physiological concentrations is mediated by parallel activation of $D_2$, $D_3$, $D_4$ and $\alpha_2$ receptors which is reproduced when endogenous dopamine levels are increased by blocking dopamine reuptake and metabolism. We provide evidence in support of dedicated spinal network components that are controlled by excitatory $D_1$ and inhibitory $D_2$ receptors that is reminiscent of the classic dopaminergic indirect and direct pathway within the striatum. These results indicate that network state is an important factor that dictates receptor-specific and therefore dose-dependent control of neuromodulators on spinal network output and advances our understanding of how neuromodulators regulate neural networks under dynamically changing excitability.

**Keywords:** dopamine, dopamine receptors, spinal cord, rhythmicity, motor systems

**Significance statement:** Monoaminergic neuromodulation of neural networks is dependent not only on target receptors but also on network state. We studied the concentration-dependent control of spinal networks of the neonatal mouse, in vitro, during a low excitability state characterized by spontaneous network activity. Spontaneous activity is an essential element for the development of networks. Under these conditions, we defined converging receptor and cellular mechanisms that contribute to the diverse, concentration-dependent control of spinal motor networks by dopamine, in vitro. These experiments advance understanding of how monoamines modulate neuronal networks under dynamically changing excitability conditions and provide evidence of dedicated $D_1$ and $D_2$ regulated network components in the spinal cord that are consistent with those reported in the striatum.

## Introduction

Neuromodulators are critical for central nervous system function and diversify circuit outputs by altering synaptic and intrinsic properties [1–3]. Dopamine is a monoamine neuromodulator that is well known for action selection in vertebrates through the control of direct and indirect circuits of the basal ganglia that express excitatory $D_1$ and inhibitory $D_2$ receptors respectively (for review, see [4] and [5–7] for examples). Dopamine is also important for the regulation of spinal motor networks that control rhythmic movements including but not limited to locomotion (for review, see [8]). In larval zebrafish, phasic and tonic firing patterns of descending neurons that provide the primary source of spinal dopamine correlates with locomotor episodes and quiescence, respectively [9]. These different firing patterns can impact the cellular release of dopamine and as a consequence, the receptor subtypes it activates [10]. For example, high levels of dopamine released during phasic cell firing activate lower affinity excitatory $D_1$ receptors and promote locomotor activity, and lower levels of dopamine released during tonic activity activate higher affinity inhibitory $D_2$ receptors and suppress motor output [11]. Similarly, dopamine has dose-dependent effects on locomotor circuits in precocial species with functional swim networks [12].

We have recently demonstrated that neuromodulation of developing mammalian spinal circuits is state-dependent [13] which is consistent with work in invertebrates [14,15]. This is important in developing spinal motor networks which produce a wide repertoire of patterned outputs at birth, including locomotor activity, as a consequence of dynamically fluctuating network excitability. That being said, neonatal rodents rarely produce coordinated bouts of locomotion and in vitro preparations of isolated spinal cord require pharmacological or electrical stimulation to drive the network into a high excitability state to produce fictive walking patterns. Instead, most of the movements observed in neonatal mice are ataxic. (See Supplementary Video 1). These movements correlate with spontaneous network activity, which can be observed in vitro [16–19]. Nevertheless, the vast majority of what we know about neuromodulation of

developing mammalian spinal networks has been derived from studies on fictive locomotor activities with dopamine being predominantly excitatory when spinal networks are operating in this state [20–31].

Based on our previous work, we hypothesized that receptor actions, and therefore concentration-dependent control of network output by dopamine, is linked to the underlying network excitability state [13]. As a result, more complex receptor-dependent actions may have been masked during high excitability states of fictive locomotion. We therefore examined how dopamine modulates spinal output at the network and cellular level of neonatal mouse spinal cords in vitro during a low excitability state characterized by spontaneous activity [16,17]. We found that the receptor-specific effects of dopamine are fundamentally different during a low excitability state compared to what has been previously reported during high excitability states. Specifically, during a low excitability state, dopamine has primarily inhibitory effects on network output acting in parallel through activation of $D_2$, $D_3$, $D_4$, and $\alpha_2$ receptors. We uncover an excitatory effect of dopamine that is likely physiologically silent. This is because endogenous dopamine levels in the spinal cord are low at this age and the excitatory effects, involving coactivation of both $D_1$ and $D_2$ receptors, require higher concentrations of dopamine. We also found that excitatory and inhibitory dopaminergic pathways act through the control of dedicated network components. Specifically, the $D_1$ pathway acts through excitation of motoneurons, likely recruiting recurrent excitatory circuits [32], with the $D_2$ pathway acting through hyperpolarization of multiple ventral interneuron subclasses. Portions of these data were presented in abstract form [33,34].

## Results

### *Dopaminergic modulation of spinal motor networks is dose-dependent and bidirectional*

We focused on the modulation of perinatal spontaneous activity patterns to investigate how dopamine modulates spinal network output during a physiologically relevant low excitability state. Using the same experimental set-up as Sharples et al. [23], we recorded spontaneous motor activity with extracellular suction electrodes from single ventral roots of the second or fifth lumbar (L2/L5) segments simultaneously from two or four spinal cord preparations sharing the same chamber. Each preparation in this series of experiments was naïve to dopamine exposure and received only a single dose of its respective concentration. This configuration ensured consistent experimental conditions across several preparations exposed to different concentrations of dopamine. Low concentrations of dopamine (1–30 μM) consistently suppressed spontaneous motor activity, whereas higher concentrations (100–300 μM) excited spontaneous motor activity, evoking episodic and continuous rhythmic patterns (Fig. 1; $n = 42$, $F_{(5,36)} = 10.5$. $p < 0.001$).

### *Parallel actions of $D_2$, $D_3$, $D_4$, dopamine and alpha-2 adrenergic receptors mediate dopaminergic inhibition of spontaneous activity*

To delineate receptor contributions to dopamine's bidirectional effects on endogenous spontaneous activity in isolated spinal cord preparations, we used antagonists selective for the family of dopamine receptors. At low concentrations of dopamine, we observed a negative response ratio (Fig. 2A, Di), which was due to a reduction in the number (Fig. 2Dii), but not the amplitude, of spontaneous episodes (Fig. 2Diii). In contrast to our hypotheses, the inhibitory effect of dopamine at low concentrations (10 μM) was not altered by antagonists targeting $D_2$ (L-741,626; $n = 3$, response ratio = $-0.57 \pm 0.26$ ), $D_2/D_3$ (sulpiride; 20 μM; $n = 10$, response ratio = $-0.36 \pm 0.2$), $D_3$ (SB-27701-A, 5 μM; $n = 3$; response ratio = $-0.36 \pm 0.3$), $D_4$ (L-745,870; $n = 3$, response ratio = $-0.32 \pm 0.1$) or $D_1/D_5$ receptors (SCH 23390; $n = 4$, response ratio = $-0.43 \pm 0.2$). However, when all $D_2$-like receptors were blocked with a cocktail of

69 sulpiride ($D_2/D_3$, 20 μM) and L-745,870 ($D_4$, 5 μM), response ratios indicated that the inhibitory effect of
70 10 μM dopamine was attenuated, compared with dopamine alone (Fig. 2C; n = 6; one-way analysis of
71 variance (ANOVA), $F_{(4,32)} = 7.3$, $p < 0.001$; Tukey post hoc $p = 0.09$), to a level where it was not
72 significantly different from a time-matched vehicle control (Fig. 2C, Di.; n = 6, $F_{(4,32)} = 7.3$, $p < 0.001$;
73 Tukey post hoc, $p = 0.98$). Burst analysis revealed no difference in the number or amplitude of episodes
74 when antagonists were present, compared with baseline (Fig. 2Dii, Diii; two-way ANOVAs for number,
75 $F_{(2,28)} = 9.5$, $p < 0.0001$; two-way ANOVA for amplitude: $F_{(4,28)} = 3.4$, $p = 0.023$). Together these data
76 suggest that the inhibitory actions of dopamine depend on parallel action of $D_2$, $D_3$ and $D_4$ receptors.
77
78 We considered the possibility that the inhibitory influence of low dopamine concentrations was partly due
79 to the activation of non-dopamine receptors. Previous work conducted in our laboratory showed that
80 dopamine inhibits cauda equina-evoked locomotion, partially via $\alpha_2$-adrenergic receptors [30]. The
81 remaining minor inhibitory effect of dopamine at 10 μM was blocked by antagonizing the $\alpha_2$-adrenergic
82 receptors with yohimbine (4 μM) in the presence of $D_2/D_3$ and $D_4$ receptor antagonists. We observed
83 significantly different response ratios, compared with 10 μM dopamine alone (Fig. 2Di; n = 6, $F_{(4,32)} =$
84 $7.3$, $p < 0.001$; Tukey post hoc, $p = 0.006$). Low dopamine concentrations did not change the number or
85 amplitude of episodes in the presence of these antagonists, compared with baseline (Fig. 2Dii, Diii)
86 suggesting that non-dopamine receptors also contribute to dopamine's inhibitory effects.
87
88 ***$D_1$ - $D_2$ receptor coactivation contributes to dopaminergic excitation of spinal network activity***
89 Dopamine binding to $D_1$ and $D_2$ heteromers can lead to depolarization via an increase in intracellular
90 calcium levels, mediated by the enzyme phospholipase C (PLC) [35–38]. Thus, we first tested the role of
91 the lower affinity $D_1$ receptor system and then examined whether the $D_2$ receptor system has a
92 cooperative role in the control of spontaneous activity. With the addition of dopamine at high
93 concentrations (i.e., 50 & 100 μM), spontaneous activity patterns became rhythmic, often producing a

94 slow rhythm with episodes of high frequency rhythmic activity. Moreover, the presence of the $D_1$-like
95 receptor antagonist, SCH-23390, reduced this effect (Fig. 3; 100 μM dopamine with 10 μM SCH-23390;
96 n = 5; response ratio, $F_{(5,35)} = 11.4$, $p < 0.001$); fast rhythm power, $F_{(4,27)} = 12.6$, $p < 0.001$; slow rhythm
97 power, $H_{(4)} = 12.8$, $p = 0.013$; Fig. 3 B & C, 50 μM dopamine with 10 μM SCH-23390; response ratio,
98 $F_{(5,35)} = 11.4$, $p < 0.001$; fast rhythm power, $F_{(4,27)} = 12.6$, $p < 0.001$; slow rhythm power, $H_{(4)} = 12.8$, $p =$
99 $0.013$, Dunn's post hoc: $p = 0.03$; one way ANOVA used in tests). These results suggest that the
100 excitatory effects of dopamine are primarily mediated by the $D_1$-like receptor family.
101
102 If $D_2$ receptors form heteromers with $D_1$ receptors, we would expect that antagonists would inhibit, rather
103 than excite responses. We tested this idea by administering $D_2$-like antagonists (sulpiride + L745,870) and
104 found that the power of the fast rhythm elicited by dopamine at 100 μM was reduced (Fig. 3 Aiii, Biii,
105 Cii; n = 4; $F_{(4,27)} = 12.6$, $p < 0.001$) to the same extent as the $D_1$-antagonist, with no effect on the power of
106 the slow rhythm (Fig. 3Ciii; $H_{(4)} = 12.8$, $p = 0.013$; Dunn's post hoc, $p = 1.0$). This suggests that $D_2$
107 receptors may contribute to the excitatory effects of dopamine.
108
109 To explore the interaction and co-activation profile of $D_1$ and $D_2$ receptors in isolated neonatal spinal
110 cords, we performed co-immunoprecipitation for $D_1$ and $D_2$ receptors and used agonists to activate both
111 receptor subtypes. After immunoprecipitating $D_2$ receptors from neonatal spinal cord lysates, we used an
112 antibody to probe for $D_1$ receptors. We detected $D_1$ receptor protein within the $D_2$ receptor
113 immunoprecipitates (Fig. 4Ciii) and these bands were blocked when pre-incubated with an antigen-
114 blocking peptide. This result indicates that $D_1$ and $D_2$ receptors form a protein complex in neonatal mouse
115 spinal cords.
116
117 In support of this idea, co-application of the $D_1$ agonist SKF 81297 (50 μM) and the $D_2$ agonist quinpirole
118 (50 μM) elicited a more robust depolarization of the ventral root DC potential, compared with 50 μM of
119 the $D_1$ agonist alone (Fig. 4A, Ci; $D_1$, n = 8; $D_1/D_2$, n = 8; one-way ANOVA $F_{(2,21)} = 5.2$, $p = 0.01$; Tukey

post hoc: $p = 0.02$). We observed no difference in the amount of spontaneous network activity evoked with co-application of a $D_2$ agonist, compared with application of the $D_1$ agonist alone, as indicated by the response ratio (Fig. 4B, Cii; one-way ANOVA, $F_{(3,29)} = 12.0$, $p < 0.001$; Tukey post hoc, $p = 0.5$). In contrast, lower concentrations of the same agonists (10 μM) produced no effects ($n = 8$ for each condition; DC potential, $t_{(6)} = 0.73$, $p = 0.24$; response ratio, $t_{(6)} = 0.9$, $p = 0.19$). Thus, consistent with previous reports for striatal neurons [36], we found a dose-dependent effect of dopamine agonists wherein co-applying high doses, but not low doses, of $D_1$ and $D_2$ receptor agonists, produced more robust depolarization than a $D_1$ agonist alone.

In addition to co-applying separate $D_1$ and $D_2$ agonists, we tested co-activating $D_1$ and $D_2$-like receptors with the $D_1/D_2$ co-agonist SKF 83959 (50 μM) [38,39]. As predicted, the co-agonist elicited a more robust depolarization of the ventral root DC potential, compared with the $D_1$ agonist, when applied alone (Fig. 4A, Ci; D1, $n = 8$; $D_1/D_2$, $n = 8$; one-way ANOVA, $F_{(2,21)} = 5.2$, $p = 0.01$; Tukey post hoc, $p = 0.03$). Interestingly, the co-agonist also robustly facilitated superimposed spontaneous activity, as indicated by a larger response ratio than co-application of the $D_1$ and $D_2$ agonists produced (Fig. 4B, Cii; one-way ANOVA, $F_{(3,29)} = 12.0$, $p < 0.001$; Tukey post hoc, $p = 0.004$). These data suggest that under certain conditions, $D_2$ receptors that are typically inhibitory can play an excitatory role via $D_1/D_2$ co-activation and contribute to lumbar motor network excitation in the neonatal mouse spinal cord.

***Low levels of endogenous spinal dopamine inhibit spontaneous activity***

We next examined how the endogenous dopamine system regulates perinatal spinal network function. Endogenous levels of dopamine were increased by blocking the dopamine transporter (DAT) with an antagonist GBR 12909 (10 μM). Blocking DAT ($n = 8$ preparations) produced a modest but significant reduction in spontaneous activity compared to time-matched vehicle controls, reflected by a reduced response ratio (Fig. 5A, Bi; one-way ANOVA, $F_{(2,19)} = 18.0$, $p < 0.001$) and a reduced number of

145 spontaneous episodes (Fig. 5Bii; n = 8, two-way ANOVA, $F_{(2,20)} = 11.8$, $p = 0.0004$), with no change in
146 amplitude (Fig. 5Biii; n = 6, two-way ANOVA, $F_{(2,20)} = 1.3$, $p = 0.3$). We questioned whether
147 extracellular dopamine metabolism may have dampened the effect of the reuptake blocker, thus
148 diminishing the predicted increase in endogenous dopamine levels. Therefore, we repeated this
149 experiment in the presence of bifemelane, a monoamine oxidase A & B inhibitor. Under these conditions,
150 we found further reductions in spontaneous activity when DAT was blocked, as indicated by a
151 significantly reduced response ratio (Fig. 5Bi; n = 6, one-way ANOVA, $F_{(2,19)} = 18.0$, $p < 0.001$). Burst
152 analysis revealed significantly fewer episodes (Fig. 5Bii; n = 6, two-way ANOVA, $F_{(2,20)} = 11.8$, p =
153 0.0004) with no change in amplitude (Fig. 5Biii; n = 6, two-way ANOVA, $F_{(2,20)} = 1.3$, $p = 0.3$).
154
155 We followed these experiments up with high-performance liquid chromatography (HPLC) to verify
156 endogenous levels of dopamine. In P3 lumbar spinal cords (n = 11) we detected low levels of dopamine;
157 in P60 adults (n = 17) we detected a threefold increase in dopamine levels (Fig. 5Biv; Mann–Whitney U =
158 10.0, T = 76, $p < 0.001$). Thus, our in vitro experiments indicated that low levels of endogenous dopamine
159 play a role in $D_2$-mediated inhibition.
160
161 ***$D_1$ receptor activation increases motoneuron excitability by reducing afterhyperpolarization properties***
162 In the next set of experiments, we were interested in determining the cellular mechanisms that mediate
163 dopamine's complex modulatory effects on spinal network output. As integrators of premotor network
164 activity that generate many of the rhythmic outputs of the spinal cord, motoneurons are ideally suited to
165 amplify spontaneous activity and respond to dopaminergic modulation. Given that they not only serve as
166 the final output for spinal networks, but they also participate in the generation of rhythmic activity [40],
167 we initially selected motoneurons as a locus for determining the cellular mechanisms for dopaminergic
168 excitation and inhibition. We made whole-cell patch-clamp recordings from 75 motoneurons (across 42
169 animals). Some of these motoneurons (n = 18 across seven animals) were filled with fluorescein-

170 conjugated dextran amine (FITC; Molecular Probes, Inc., Eugene Oregon) and verified post hoc using
171 immunohistochemistry for the presence of choline acetyltransferase (ChAT; Fig. 6A). One hundred
172 percent of filled cells were ChAT positive indicating that we were indeed recording from motoneurons.
173 Electrical properties measured in a group of these cells (n = 8 cells across five animals) were comparable
174 to cells from putative motoneurons recorded in the remaining experiments (Table 1) indicating that these
175 cells are also likely motoneurons. Motoneurons also display characteristic time-dependent changes in
176 repetitive firing frequency during sustained depolarizing current injections (Fig. 6 Cii) [41–43]. We found
177 that all but two cells demonstrated a time-dependent reduction in firing rate throughout the duration of a
178 0.5 s depolarizing current injection, as indicated by the ratio between maximum steady-state and first
179 spike interval frequencies. This phenomenon is known as spike frequency adaptation (SFA; mean SFA
180 ratio = 0.47 ± 0.19). In addition, doublet firing occurred at the onset of repetitive firing in 5 cells (8%).
181
182 Consistent with previous reports from our laboratory [44,45] and with our network recordings in this
183 report, 100 μM of dopamine increased motoneuron excitability (n = 5 cells across four animals); we
184 reproduced this effect with the $D_1$ agonist SKF 81297 (20 μM; n = 8 cells across five animals). Both 100
185 μM dopamine and the $D_1$ agonist depolarized the membrane potential (Fig. 6Bi; $H_{(2)} = 18.9$, $p < 0.001$),
186 increased negative holding current (vehicle, −7.1 ± 33 pA; DA, −247 ± 78 pA; $D_1$, −174 ± 49 pA; $H_{(2)} =$
187 $18.9$, $p = 0.001$) and input resistance (Fig. 6Bii; $H_{(2)} = 16.0$, $p < 0.001$), and decreased rheobase (Fig. 6Bii;
188 $F_{(2,22)} = 5.0$, $p = 0.016$) beyond that of the time-matched vehicle control. We found no change in spike rise
189 time ($F_{(2,22)} = 1.0$, $p = 0.4$) or half width ($F_{(2,22)} = 0.8$, $p = 0.5$). The $D_1$ agonist reduced the amplitude of
190 the afterhyperpolarization (AHP); however, 100 μM dopamine did not reduce AHP amplitude beyond
191 that of a time-matched vehicle control (Fig 6Biv; $F_{(2,22)} = 7.7$, $p = 0.003$). Frequency–current (FI)
192 relationships were measured for steady state and first spike interval during a series of depolarizing current
193 pulses (Fig. 6Ci). Both 100 μM dopamine and the $D_1$ agonist reduced the latency to first spike beyond
194 that of the time-matched vehicle control (Fig. 6Cii; $F_{(2,17)} = 9.6$, $p = 0.002$). Dopamine (100 μM) and the
195 $D_1$ agonist increased the slope of the exponential region of the FI relationship for the first spike interval

196 (Fig. 6Di–Dii; $F_{(2,22)} = 8.4$, $p = 0.002$) and reduced the slope of the steady-state FI relationship (Fig.
197 6Diii–Div; $H_{(2)} = 9.4$, $p = 0.009$). The reduction in steady-state slope was due to a leftward shift in steady-
198 state FI relationship (Fig. 6Diii) characterized by a reduction in the threshold for repetitive firing (Fig.
199 6Ciii; $H_{(2)} = 14$, $p < 0.001$) with no change in the maximum steady-state firing rate ($H_{(2)} = 1.4$, $p = 0.5$).
200 These results indicate that activation of $D_1$ receptors elicit consistent effects as high concentrations of
201 dopamine on motoneuron excitability and is a likely mechanism contributing to dopaminergic excitation
202 of motor output.
203

204 ***Dopaminergic inhibition through $D_2$ - receptor hyperpolarization of distributed populations of ventral***
205 ***interneurons***

206 We next set out to determine the cellular mechanisms that mediate the inhibitory effects of dopamine on
207 spinal network output with motoneurons as our first target. In contrast to our network recordings, low
208 concentrations of dopamine (1–10 μM; n = 20 cells across 14 animals; Table 1) and the $D_2$ agonist
209 quinpirole (20 μM; n = 12 cells across seven animals; Table 1) did not alter any passive, spike or
210 repetitive firing properties of motoneurons beyond that of the time-matched vehicle control (n = 12 cells
211 across six animals). A lack of responsiveness was not due to the diversity of motoneurons as there was no
212 correlation between cell capacitance and changes in membrane potential or holding current elicited by
213 low concentrations of dopamine ($r = -0.3$, $p = 0.13$) or quinpirole ($r = -0.1$, $p = 0.72$). These results
214 suggest that the inhibitory actions of dopamine on spinal network output are not due to $D_2$-receptor
215 inhibition of intrinsic motoneuron excitability; instead, dopamine may be acting on premotor
216 interneurons.
217

218 Many of the premotor interneurons that produce the rhythmic activities generated by the spinal cord are
219 distributed across lamina's VII - X of the ventral lumbar spinal cord. We next recorded from ventral
220 interneurons located in lamina VII–X to determine a cellular locus for $D_2$-mediated inhibition of spinal

221 network output (n = 30 cells across 17 animals; Table 2). Quinpirole produced a sustained
222 hyperpolarization of the resting membrane potential in 33% of interneurons (Fig. 7B, C, Di; n = 10; dVm
223 = −4.8 ± 2.4 mV; two-way ANOVA, $F_{(2,37)} = 26.1$, $p < 0.0001$) and a transient hyperpolarization of
224 membrane potential in 10% of interneurons (n = 3; dVm = −5.16 ± 1.9 mV) that persisted for 209 ± 108 s
225 before returning to baseline levels. The change in resting membrane potential was greater in the
226 responders compared to non-responders (dVm responders = - 4.8 ± 2.4 mV; dVm non-responders = 1.6 ±
227 1.9 mV; unpaired t-test $t_{(28)} = 7.8$, $p < 0.0001$). Quinpirole reduced the input resistance (Fig. 7Dii; two-
228 way ANOVA, $F_{(2,37)} = 4.1$, $p = 0.025$) and increased the spike rise time (Fig. 7Div; two-way ANOVA,
229 $F_{(2,35)} = 5.2$, $p = 0.01$; Dunn post hoc test, p=0.02) but not the half width ($F_{(2,35)} = 2.6$, $p = 0.086$) in the
230 group of responding interneurons ("responders"). For both responders and non - responders, quinpirole
231 did not alter rheobase (Fig. 7Diii; two-way ANOVA, $F_{(2,37)} = 0.5$, $p = 0.6$), action potential threshold
232 (two-way ANOVA, $F_{(2,37)} = 0.3$, $p = 0.7$), AHP amplitude (two-way ANOVA, $F_{(2,37)} = 0.04$, $p = 0.96$),
233 duration (two-way ANOVA, $F_{(2,37)} = 0.8$, $p = 0.45$), threshold for repetitive firing (two-way ANOVA,
234 $F_{(2,37)} = 0.01$, $p = 0.98$), maximum steady-state firing rate (Fig. 7Dvi; two-way ANOVA, $F_{(3,37)} = 0.8$, p =
235 0.5 ) or steady-state FI slope (Fig. 7Dv: two-way ANOVA, $F_{(2,37)} = 0.9$, $p = 0.4$). The capacitance (two-
236 way ANOVA, $F_{(2,37)} = 4.2$, $p = 0.02$) and holding current (two-way ANOVA, $F_{(2,37)} = 4.9$, $p = 0.02$) were
237 higher in responders than in non - responders (Table 2) and a greater proportion of responders were
238 localized to more medial regions of spinal slices (Fig. 7B), where putative commissural interneurons
239 reside [46].
240
241 We next set out to determine the type of interneurons that were hyperpolarized by quinpirole. Given that
242 many of the responding cells were located medially, we next targeted descending commissural
243 interneurons (dCINs; n = 10 cells across five animals; Table 2) since this population can be identified
244 based on anatomical connectivity [47,48], display intrinsic burst properties [49] and are rhythmically-
245 active during neurochemically-evoked fictive locomotion [50]. dCINs were retrogradely labelled with
246 tetramethylrhodamine-conjugated dextran amine (molecular weight (MW) 3000; Molecular Probes, Inc.)

247 inserted into the ventrolateral funiculus at the L4 segment (Fig. 7A). In contrast to our hypothesis, only
248 one dCIN responded with a sustained hyperpolarization and two were transiently hyperpolarized (Fig. 7B)
249 by quinpirole. Quinpirole did not alter any passive, spike, or repetitive firing properties of dCINs (n = 10;
250 Fig. 7D). These data suggest that the dCINs, although responsive in similar proportions to our global
251 interneuron survey, do not exclusively account for the 33% responding group and, therefore, are likely,
252 not responsible for the observed network effects. Interestingly, when all interneuron data were pooled (n
253 = 40 cells), irrespective of responsiveness as indicated by changes in resting membrane potential,
254 quinpirole had the greatest effect in cells that had a higher maximum steady-state firing rate at baseline
255 (Fig. 7DViii; $r = -0.37$, $p = 0.026$). There was no correlation between baseline FI slope and changes in FI
256 slope in response to quinpirole ($r = -0.09$, $p = 0.6$).
257
258 While dCINs can be identified anatomically, they are heterogeneous with respect to their neurotransmitter
259 phenotype [51] and as a result have varying contributions to network activities [46,50,52]. We therefore
260 next targeted V3 interneurons which are exclusively glutamatergic, contribute to the stabilization of
261 locomotor-like rhythmicity and can be identified genetically based on the expression of the Sim1
262 transcription factor [53]. Heterogeneity with respect to location, morphology and electrophysiological
263 properties has also been reported in V3 interneurons [54,55] which may be accounted for in part by a
264 recently described hierarchical microcircuit whereby a medial population projects to a lateral population
265 which provide glutamatergic excitation of ipsilateral motoneurons. Both populations also project
266 commissurally and receive recurrent glutamatergic inputs from intra and intersegmental ipsilateral
267 motoneurons [32]. Given that dopamine inhibits ventral root-evoked locomotor activity, which may be
268 mediated by this circuit [56], through $D_2$-receptor signaling [31], we hypothesized that V3 interneurons
269 may be a cellular locus for $D_2$-mediated inhibition of spinal network activity.
270
271 Consistent with our global interneuron survey, quinpirole produced a sustained hyperpolarization of the
272 resting membrane potential in a proportion of V3 interneurons (n=5 cells; 27%) that we recorded from

273 (total V3 interneurons n=23 cells, 7 animals) and transient hyperpolarization in 3 (13%) V3 interneurons.
274 The magnitude of the response in the 5 cells that responded with a sustained hyperpolarization was
275 variable and approached, but did not reach, significance (Supp Figure 1; paired t-test: $t_{(4)}= 2.5$, $p = 0.06$);
276 however, did reach significance when the cells that responded with a transient hyperpolarization were
277 included in the analysis (paired t-test: $t_{(6)} = 2.7$, $p = 0.03$). Consistent with our global interneuron survey
278 the change in resting membrane potential elicited by quinpirole was significantly greater in responding (n
279 = 5; dVm = -1.9 ± 1.9 mV) compared to non-responding (n = 15; dVm = -0.3 ± 1.0 mV) V3 interneurons
280 (unpaired t-test: $t_{(16)} = 3.8$, $p = 0.002$).
281

## Discussion

Dopamine is a monoamine neuromodulator that is important for the control of rhythmically active motor circuits across phyla (reviewed by [8]) but is probably best known in vertebrates for the control of dedicated circuits in the basal ganglia that control action selection (reviewed by [57] ). Work in small circuits of invertebrates has established that circuit connectomes define the constraints on which networks operate and that neuromodulators diversify outputs by altering intrinsic and synaptic properties of the neurons that compose the circuit (for reviews see [1–3]. In line with this, the distribution of receptors within circuits constrain the effect of neuromodulators on circuit output. For example, dopamine is exclusively inhibitory in spinal circuits of *Xenopus* tadpoles prior to free-swimming stages [58] due to expression of $D_2$ but not $D_1$ receptors. We show that dopamine has bidirectional concentration-dependent effects on spinal network output in neonatal mice where all dopamine receptor types are expressed which is consistent with what has been reported in tadpoles at free swimming-stages [12]. Our data highlights that neuromodulator concentration is also important because receptors have varying ligand affinities which underlie concentration-dependent actions of modulators. Although dopamine predominantly inhibits spinal output in neonatal mice, similar to pre-free-swimming tadpoles, it is primarily due to the concentration of spinal dopamine, not the distribution of receptors. Our previous work shows that neuromodulation of mammalian spinal networks is dependent on network excitability state [13] which is consistent with findings from invertebrates [14,15]. Our current work shows that receptor mechanisms and concentration-dependent control of spinal network output is also state-dependent. This is important because receptor expression, modulator concentration and network excitability are not fixed and fluctuate dynamically [59,60]. Therefore, these three factors need to be considered if we wish to understand how networks create diverse neuromodulator-dependent outputs (Figure 8A).

### *A physiologically silent excitatory $D_1$ pathway?*

Previous work has shown predominantly excitatory $D_1$-receptor mediated effects of dopamine on fictive locomotion which is characteristic of the network operating in a high excitability state [13] - albeit in

307 these studies, higher concentrations of dopamine are necessary to elicit observable effects [20–25]. Here,
308 we show that endogenous levels of dopamine within the spinal cord of neonatal mice are low. Even
309 though HPLC suggests low concentrations of dopamine in the neonatal spinal cord, a critical question that
310 we addressed is what would happen when we manipulated endogenous dopamine? We accomplished this
311 by blocking dopamine reuptake and metabolism and found that the effects were not excitatory, but
312 inhibitory. Based on this, we suggest that although present, the excitatory $D_1$-mediated pathway is
313 'physiologically silent' during early postnatal stages given that endogenous levels are not sufficient to
314 activate this pathway. A similar phenomenon has been reported for glutamatergic synapses in developing
315 circuits of the hippocampus which express NMDA but not AMPA receptors. As a result, glutamatergic
316 synapses fall 'physiologically silent' as the release of glutamate does not produce sufficient
317 depolarization of the postsynaptic membrane to remove the magnesium block from the pore of the
318 NMDA channel [61,62].
319
320 Excitability state also influences the receptor mechanisms and therefore concentration-dependent control
321 of modulators on network output. In the spinal cord, $D_1$ pathways may be more important for the
322 regulation of spinal circuits operating in higher excitability states. For example, fictive locomotor rhythms
323 are drastically impacted when $D_1$ receptors are manipulated whereas manipulation of $D_2$ receptors elicit
324 only subtle changes in rhythm frequency, with rhythm robustness being maintained [23] (Figure 8Bii.). In
325 the adult animal; however, network excitability increases, and spinal dopamine levels are higher due to
326 increases in descending inputs. In line with this, optogenetic activation of the dopaminergic A11 leads to
327 an increase in motor activity [63]. Similarly, the excitatory $D_1$ system is more important for the control of
328 stepping movements whereas the inhibitory $D_2$ system plays less of a role [22,64]. Instead, the inhibitory
329 $D_2$ pathway may be more important in maintaining network quiescence during periods of immobility such
330 as has been inferred by the study of firing patterns in the zebrafish [9]. Our data demonstrates that in the
331 neonatal mouse, where spinal dopamine levels and network excitability are low, that inhibition of motor
332 output prevails (Figure 8Bii.). Thus, this points to the receptor-specific and therefore concentration-

333 dependent control of modulators on network output being strongly influenced by the state of the network
334 on which they are acting.
335
336 ***Dedicated network components segregate excitatory and inhibitory control of spinal networks***
337 Dedicated circuits regulated by non-overlapping populations of neurons that express $D_1$ and $D_2$ receptors
338 compose the direct and indirect pathways of the basal ganglia in vertebrates and have also been reported
339 in the superior colliculus of rodents [65]. Our work suggests dedicated network elements within the spinal
340 cord that are regulated by $D_1$ and $D_2$ pathways (Figure 8Biii.). Specifically, we found that $D_1$ receptors
341 excite motoneurons through similar mechanisms that have been previously reported [44,45], but are not
342 affected by low concentrations of dopamine or $D_2$ agonists. This points to the possibility of a dedicated
343 $D_1$-dependent circuit that could underlie the generation of rhythmic activities elicited by high
344 concentrations of dopamine. Motoneurons compose key rhythm generating elements in invertebrate
345 circuits [66–68] and also participate in rhythm generation in vertebrates [69], including rodents
346 [32,40,56,70,71]. V3 interneurons are one subclass of genetically-defined spinal interneuron that are
347 important for the generation of rhythmic activities in mammalian spinal networks [53,55,72] and receive
348 recurrent excitatory collaterals from motoneurons in rodents [32]. Motoneurons in the rodent spinal cord
349 also form glutamatergic synaptic connections amongst each other [71] and activation of $D_1$ receptors
350 could serve to synchronize motor pools. Previous results demonstrating $D_1$- and not $D_2$-mediated
351 increases in AMPA conductances on motoneurons [45] support this possibility. We cannot rule out the
352 possibility that there is a degree of overlap between $D_1$ and $D_2$ controlled network elements within the
353 spinal cord. While we did not examine the $D_1$ control of ventral interneurons, we did find that $D_2$
354 receptors hyperpolarize a subset of V3 interneurons. This population is therefore a potential cellular locus
355 where cooperative excitatory $D_1$-$D_2$ interactions that we report here could occur. $D_1$ and $D_2$ receptors have
356 been reported in the brain to become co-activated or form heterodimeric complexes that augment
357 neuronal excitability through PLC-dependent increases in intracellular calcium [35–38]. Our
358 pharmacological and immunoprecipitation data indicate that this may also occur in the neonatal mouse

359 spinal cord. Although this pathway may be physiologically silent during early postnatal development,
360 increasing dopamine concentrations at later stages may activate this pathway.
361
362 The inhibitory $D_2$ pathway on the other hand does not appear to act through the modulation of
363 motoneuron intrinsic or synaptic properties [45] but instead hyperpolarizes a proportion of ventral
364 interneurons. Based on our responsiveness criteria, a majority of cells that responded to a $D_2$ agonist with
365 sustained hyperpolarization of the membrane potential were localized more medially in lumbar slices. We
366 tested the hypothesis that a subpopulation of interneurons was $D_2$ sensitive and tested both dCINs and
367 genetically identified V3 interneurons. Our hypothesis was not supported, and similar proportions of $D_2$
368 sensitive neurons were found; however, the data suggest that there is heterogeneity in the responsiveness
369 to neuromodulators within a class of genetically defined interneurons and that $D_2$ actions may not be
370 localized to a particular class of interneurons. One possibility is that neuromodulators elicit a robust effect
371 on network output through distributed control across multiple classes of genetically-defined interneurons
372 which would be consistent with findings that the locomotor rhythm generator is also distributed across
373 several classes of interneurons [73–75]. Our network data suggests that low concentrations of dopamine
374 inhibit network output by acting in parallel on $D_2$, $D_3$, $D_4$ and $\alpha_2$ receptors. We may therefore have
375 underestimated the cellular targets that underlie dopamine's robust inhibitory effect on the network given
376 that in this series of experiments we looked at the activation of $D_2$ receptors alone.
377

378 ***Developmental considerations for the endogenous dopaminergic system***

379 This robust inhibitory system may act as a brake on network activity during perinatal development when
380 chloride-mediated synaptic transmission still causes partial depolarization [76]. An inhibitory brake
381 would prevent runaway excitation of spinal network activity during this critical period of development. A
382 robust background inhibitory system mediated by the parallel inhibitory action of $D_2$, $D_3$, $D_4$, and α2-

383 adrenergic receptors activated by low levels of endogenous dopamine would counteract depolarizing
384 chloride-mediated transmission.
385
386 Signaling through [76] $D_2$-like receptors may also play a role in driving the maturation of spinal
387 networks. In larval zebrafish, $D_4$ receptors drive the maturation of spinal locomotor network organization
388 [77] and function leading to changes in locomotor behaviour [78]. Similar processes may also occur
389 perinatally in rodents, in that the preferential activation of the $D_2$ receptor system may favour intracellular
390 signaling that results in network reorganization. Serotonin receptors have been found to shape network
391 function and inhibitory synaptic transmission during early postnatal days of rodents [79,80]. Dopamine
392 could, therefore, act analogously via the $D_2$-system during perinatal development.
393

394 ***Conclusions***

395 Here we present evidence for an inhibitory physiological role of dopamine in the regulation of developing
396 mammalian spinal networks. We also demonstrate an excitatory $D_1$-mediated pathway that acts through
397 excitation of motoneurons, and possibly recurrent excitatory collaterals to CPG neurons, however given
398 that endogenous levels of dopamine are low, propose that this pathway is physiologically silent. These
399 data advance our understanding of how neuromodulators regulate network output in light of dynamically
400 changing modulator concentrations and levels of network excitability.

401 **Methods**

402 ***Ethical approval & animals***

403 Experiments were performed on male and female neonatal (P0–P4, n = 262) and adult (P50, n = 17)
404 C57BL/6 mice. A subset of experiments were performed on spinal cord slices obtained from neonatal
405 (P0-4, n=7) *Sim1*$^{Cre/+}$; *Rosa*$^{floxstop26TdTom}$ which were used to visualize and record from V3 interneurons. All
406 procedures performed were approved by the University of Calgary Health Sciences Animal Care
407 Committee University Committee on Laboratory Animals at Dalhousie University.

408

409 ***Tissue preparation***

410 We anesthetized all animals by hypothermia. Pups were decapitated and eviscerated to expose the
411 vertebral column and rib cage. The isolated vertebrae and rib cage were transferred to a dish lined with a
412 silicone elastomer (Sylgard; DowDuPont, Midland, MI) and perfused with room-temperature (21 - 23ºC)
413 carbogenated (95% $O_2$ / 5% $CO_2$) aCSF (in mM, 4 KCl, 128 NaCl, 1 $MgSO_4$, 1.5 $CaCl_2$, 0.5 $Na_2HPO_4$, 21
414 $NaHCO_3$, 30 D-glucose; 310–315 mOsm.). We exposed the spinal cord with a ventral laminectomy and
415 isolated it by cutting the nerve roots that connected it to the vertebral column. The isolated spinal cord
416 was then transferred to a recording chamber, perfused with carbogenated aCSF, and placed ventral side
417 up. The bath temperature was gradually increased to 27°C [81]. We let the spinal cords stabilize for 1
418 hour before performing experiments.

419

420 ***Spinal cord slice preparation***

421 Following isolation, spinal cords were transected above the tenth thoracic (T10) and below the first sacral
422 (S1) segments and transferred to a slicing chamber. Pre-warmed liquefied 20% gelatin was used to secure
423 cords to an agar (3%) block that was super-glued to the base of a cutting chamber and immersed in ice-
424 cold, carbogenated, high-sucrose slicing aCSF (in mM, 25 NaCl, 188 sucrose, 1.9 KCl, 10 Mg $SO_4$, 1.2
425 $Na_2HPO_4$, 26 $NaHCO_3$; 25 D-Glucose; 340 mOsm). Using a vibratome (Leica, Bussloch, Germany) we

426 cut 250-µm-thick lumbar slices, collected and transferred them to a recovery chamber containing regular
427 carbogenated aCSF (see Tissue Preparation) heated to 32ºC for one hour, then maintained them at room
428 temperature for at least 30 minutes before transferring them to a recording chamber.
429

430 ***Labelling of descending commissural interneurons (dCINs)***

431 We retrogradely labelled dCINs by inserting tetramethylrhodamine-conjugated dextran amine crystals
432 (MW 3000; Molecular Probes, Inc.) into a cut in the ventrolateral funiculus at the L4 segment. Spinal
433 cords recovered for 4 hours to allow retrograde uptake of the fluorescent dye. Fluorescently-labelled cells
434 were visualized with epifluorescent illumination.
435

436 ***Electrophysiological recordings***

437 Extracellular neurograms were recorded by drawing ventral roots of the second (L2) and fifth (L5) lumbar
438 segments into tight-fitting suction electrodes fashioned from polyethylene tubing (PE50). Signals were
439 amplified 1000× in total via 10× pre-amplification and 100× second-stage amplification (Cornerstone
440 EX4-400 Quad Differential Amplifier; Dagan Corporation, Minneapolis, MN). Amplified signals were
441 band-pass filtered (0.1–1000 Hz) and digitized at 2.5 kHz (Digidata 1440A/1550B; Molecular Devices,
442 Sunnyvale, CA). Data were acquired in Clampex 10.4/10.7 software (Molecular Devices) and saved on a
443 Dell computer for offline analysis. All experiments were performed on spinal cords naïve to drugs and
444 experimental treatment.
445

446 ***Whole-cell patch-clamp recordings***

447 Spinal cord slices were gently transferred to a recording chamber perfused with room-temperature
448 carbogenated recording aCSF (in mM, 128 NaCl, 4 KCl, 1.5 $CaCl_2$, 1.0 $MgSO_4$, 0.5 $Na_2HPO_4$, 21
449 $NaHCO_3$, 30 D-glucose; approximately 310 mOsm) and stabilized in the recording dish with a stainless-
450 steel harp. We gradually heated aCSF to 27°C. Slices were visualized (Olympus BX51WI; Olympus

451 Corporation, Tokyo, Japan) under 5× magnification and putative motoneurons identified using a 40×
452 objective with infrared differential interference contrast (IR-DIC) illumination. We identified putative
453 motoneurons based on their location in the ventrolateral spinal cord and a soma diameter of greater than
454 20 µm. A cohort of motoneurons was passively filled with fluorescein dextran amine (FITC; MW 3000;
455 200µM; Molecular Probes, Inc.) added to the intracellular solution to visualize and localize the recorded
456 cells, for 20–60 minutes and motoneuron identity was verified post hoc by performing
457 immunohistochemistry for choline acetyltransferase (ChAT). To verify motoneuron identity in
458 subsequent experiments, basal biophysical properties of putative motoneurons were compared with the
459 FITC-filled ChAT-positive cells. We identified no differences in basal biophysical properties of ChAT-
460 positive identified cells, compared with cells in other experiments identified by position and size (Table
461 1). In one set of experiments, we recorded from ventral interneurons in lamina VII–X, descending
462 commissural interneurons (dCINs) and V3 interneurons of the lumbar spinal cord (Table 2). We measured
463 the distance of each interneuron from the central canal (LinLab2; Scientifica, Uckfield, UK) and
464 normalized position, relative to lateral and ventral borders, and plotted the normalized positions on a
465 template transverse spinal cord. Responsiveness was determined by the change in resting membrane
466 potential. All experiments were performed on one cell per slice to ensure that all cells were naïve to
467 treatment.
468
469 Recording electrodes were pulled from borosilicate capillary tubes (O.D. = 1.5mm, I.D. = 0.86 mm) using
470 a Flaming/Brown Model P-97 micropipette puller (Sutter Instrument, Novato, CA). Pipettes pulled to
471 record from motoneurons, and interneurons were within the range of 3–5 MΩ and 6–9 MΩ, respectively.
472 Pipettes were backfilled with intracellular solution (in mM, 130 K-gluconate, 0.1 EGTA, 10 HEPES, 7
473 NaCl, 0.3 $MgCl_2$, 2 ATP, 0.5 GTP, 5 phosphocreatine; 280 mOsm). Intracellular solutions were balanced
474 to a pH of 7.3 with 10 M KOH and osmolality was cross-checked to fall within the range of 275–290
475 mOsm. Data were acquired at 10 kHz using Clampex software (PClamp 10.4; Molecular Devices).
476

477 We examined intrinsic properties of motoneurons and ventral interneurons and terminated experiments if
478 access resistance was greater than 25 MΩ for motoneurons and 35 MΩ for interneurons, if cells had a
479 resting membrane potential greater than −50 mV, or if action potential amplitude was less than 60 mV at
480 baseline. Cells were excluded from analysis if access resistance deviated by more than 20% by the end of
481 the recording. We held all cells at a membrane potential of approximately −75 mV during experiments,
482 after correcting for a liquid junction potential of 14.3 mV. The liquid junction potential was calculated in
483 Clampfit (PClamp 10.4; Molecular Devices), using the ionic composition of our extracellular and
484 intracellular solutions. Protocols for the examination of intrinsic properties have been described elsewhere
485 [82].

486

487 ***Pharmacology***

488 Dopamine hydrochloride (Sigma-Aldrich, Inc., St. Louis, MO) was bath applied in separate experiments
489 at 1 μM, 3 μM, 10 μM, 30 μM, 100 μM, and 300 μM to determine dose-dependent effects on motor
490 activity. The receptor-selective agonists we used included SKF 81297 for $D_1$-like receptors (10–50 μM;
491 Tocris, Minneapolis, MN); quinpirole for $D_2$-like receptors (10–50 μM; Tocris); and the $D_1$/$D_2$ receptor
492 co-agonist SKF 83959 (10–50 μM; Tocris). For dopamine receptor antagonists we used the $D_1$-like
493 antagonist SCH-23390 (10 μM; Tocris); the $D_2$-like antagonists sulpiride (20 μM) and L-741,626 (12
494 μM); the selective $D_3$ receptor antagonist SB 27701A (5 μM; Tocris); the selective $D_4$ receptor antagonist
495 L-745, 870 (5 μM; Tocris). We also used the $\alpha_2$ adrenergic receptor antagonist, yohimbine (2–4 μM;
496 Tocris). Endogenous dopamine levels were manipulated with the DAT inhibitor GBR-12909 (10 μM;
497 Hello Bio, Princeton, NJ) and the monoamine oxidase A & B inhibitor bifemelane (50 μM; Tocris).

498

499 ***Immunoprecipitation for $D_1$ and $D_2$ receptors***

500 Spinal cords were dissected in ice-cold (4–8ºC) aCSF and homogenized in lysis buffer containing 50 mM
501 TrisHCl, 150 mM NaCl, 10 mM EDTA, 0.1% Triton-X, and 5% Glycerol. Lysis buffer contained

502 protease inhibitors (Sigma) and phosphatase inhibitors (GBiosciences). We homogenized three spinal
503 cords in 100 μL of buffer and incubated them on ice for 1 hour before centrifuging them at 10,000 rpm
504 for 30 minutes at 4ºC. Lysates were then extracted and stored at −20 ºC.
505
506 To reduce nonspecific binding, we first incubated lysates in anti-rabbit Ig agarose beads (Trueblot;
507 Rockland Inc., Limerick, PA) for 30 minutes, on ice and in the absence of primary antibody. We then
508 removed the supernatant and incubated the lysates on ice for 1 hour with rabbit antibody to $D_2$ receptors
509 (1 μg per 100 μL, Millipore). Anti-rabbit Ig IP beads were added and samples were incubated overnight at
510 4°C with gentle agitation. Immunoprecipitates were washed with lysis buffer, heated in loading buffer
511 (350 mM Tris, 30% glycerol, 1.6% SDS, 1.2% bromophenol blue, 6% β-mercaptoethanol) to 95°C for 10
512 min, electrophoresed on a precast SDS gel (4–12% Tris HCl; BioRad, Hercules, CA), and transferred
513 onto a nitrocellulose membrane. After blocking, the membranes were incubated with guinea pig antibody
514 to $D_1$ receptors (1:400; Alomone, Jerusalem, Israel) and rabbit antibody to $D_2$ receptors (1:500; Millipore,
515 Burlington, MA), washed, incubated for 2 hours at room temperature in fluorophore-conjugated
516 secondary antibodies (IRDye anti-guinea pig and Trueblot anti-rabbit IgG DyLight, 1:1000), and
517 visualized via antibody fluorescence at 680 or 800 nm (Odyssey CLx; LI-COR Biosciences, Lincoln,
518 NE).
519
520 ***Post hoc verification of motoneurons***
521 Following the completion of experimental protocols, we post-fixed slices overnight in 4%
522 paraformaldehyde (PFA) at 4ºC, washed them the next morning in phosphate-buffered saline (PBS) for
523 three 20-minute intervals, and stored them at 4ºC. On the day we performed immunohistochemistry, we
524 first washed the slices for 30 minutes (3 × 10 minutes) in PBS with 0.5% Triton-X 100 (PBST) then
525 incubated them at room temperature (21 -23ºC) for 6 hours in blocking solution containing 10% donkey
526 serum in 0.5% PBST. Primary antibodies for choline acetyltransferase (ChAT) (1:500; goat anti-ChAT;

527 Millipore Cat No. AB144) and the fluorescence marker (1:1000; rabbit anti-FITC, ThermoFisher Cat No.
528 11090) were diluted in blocking solution and the slices incubated with them for at least 24 hours at room
529 temperature. Slices were then washed in PBST (0.5%) for 80 minutes (4 × 20 min) at room temperature
530 before secondary antibodies (donkey anti-rabbit Alexa Fluor 1:1000, Life Technologies Cat No. A-21206;
531 Donkey anti-Goat Alexa 568 1:1000; Cat No. A21447, Life Technologies, Carlsbad, CA) were applied
532 for 4–8 hours at room temperature, then washed for 80 minutes in PBST (0.5%). Slices were mounted and
533 coverslipped with fluorescent mounting medium (Vectashield; Vector Laboratories, Burlingame, CA);
534 coverslips were separated from slides by 500 µm spacers to prevent crushing.
535

536 ***Imaging***

537 All sections processed via immunohistochemistry were imaged on a Nikon A1R MP$^+$ microscope (Nikon,
538 Tokyo, Japan) operating in confocal mode with a 16× water-immersion objective lens (numerical aperture
539 [NA] = 0.8, working distance [WD] = 3 mm). Image acquisition used a z-step of 1 µm and averaged two
540 frames with a resolution of 2048 × 2048. Pixel dwell time was 2.5 ms and exposure settings were
541 maintained for all sections. We used NIS-Elements software (Nikon) for image acquisition and ImageJ to
542 perform maximum intensity projections of z-stacks.
543

544 ***High-performance liquid chromatography***

545 Monoamine content of neonatal and adult spinal cords was measured using high-performance liquid
546 chromatography (HPLC). We dissected spinal cords from neonatal (P3, n = 11) C57BL/6 mice in aCSF as
547 described above and extracted adult spinal cords (P60, n = 17) with a pressure ejection method. Tissue
548 was then flash-frozen with liquid nitrogen, stored at −80ºC, and analyzed for biogenic amines with a
549 modified version of the Parent et al. HPLC method [76]. Tissue was homogenized in ice-cold 0.1 M
550 perchloric acid. We centrifuged the homogenate and used 10 µl of supernatant in the assay, employing an
551 Atlantis dC18 column (Waters, Milford, MA) and an electrochemical detector.

552 ***Data analysis***

553 We determined the relative inhibitory or excitatory effects of dopamine and dopamine receptor agonists
554 on spontaneous motor network activity using methods similar to those in our previous work [23]: we
555 calculated a response ratio from single ventral root neurograms between the root mean square of 5
556 minutes of basal spontaneous activity and 5 minutes of activity recorded 20 minutes after adding the drug.
557 We subtracted 1 from the response ratio so that positive values reflect excitation and negative values
558 reflect inhibition. The response ratio was used as a high throughput assay to detect global changes in
559 network activity. Neurogram data were analyzed with Spike2 software. Bursts of spontaneous activity
560 were analyzed using Clampfit (Molecular Devices) to determine how episode number and amplitude
561 contributed to changes in response ratio. Spectral analyses were conducted using Spinalcore software [83]
562 whenever we detected excitatory changes or observed rhythmicity.

563

564 Patterns of rhythmic motor activity recorded from single ventral roots were analyzed with autowavelet
565 spectral analysis. We created and analyzed frequency–power spectrograms by selecting regions of interest
566 around frequency ranges that coincided with those in the raw neurogram. The spectrograms revealed two
567 high power regions that reflect distinct rhythms evoked by dopamine at high concentrations: a slow 0.01–
568 0.04 Hz rhythm and a fast 0.8–1.2 Hz rhythm. Regions of interest were selected within these frequency
569 ranges and analyzed over the time course of each experiment. Frequency power within selected regions of
570 interest that corresponded to the fast and slow rhythms were used as a measure of rhythm robustness.
571 Data were segmented into 30 s bins and averaged over 5-minute intervals for statistical analysis. We used
572 tools available in Spinalcore for all analyses of rhythmic motor activity [83], consistent with Sharples
573 and Whelan [13].

574

575 Motoneuron and interneuron intrinsic properties measured during whole-cell patch-clamp experiments
576 were analyzed as in our previous work [82,84], with the exception of repetitive firing analyses, which
577 examined the instantaneous firing rate for the first spike interval and steady-state firing separately.

578 ***Experimental design and statistical analysis***

579 All experiments were repeated measures. We tested for differences in the magnitude of effects between
580 conditions with one-way ANOVAs, focusing on comparisons to time-matched vehicle controls. Two-way
581 ANOVAs compared baseline to multiple post-drug conditions. All effects surpassing a significance
582 threshold of $p < 0.05$ were further examined with post hoc analyses. We used Holm-Sidak post hoc tests
583 to compare all treatment conditions to the appropriate normalized time-matched vehicle control. Data that
584 violated assumptions of normality (Shapiro–Wilk test) or equal variance (Brown–Forsythe test) were
585 analyzed via nonparametric Mann–Whitney *U* (if two groups) or Kruskal–Wallis (if more than two
586 groups) tests.

**Tables and Captions**

***Table 1: Baseline motoneuron intrinsic properties.***
Passive, spike, and repetitive firing properties of motoneurons with dopamine or dopamine agonists did not differ at baseline in this series of experiments. Motoneuron identity was verified in a subset of experiments where cells were filled with fluorescein and verified post hoc for expression of choline acetyltransferase (ChAT); 100% of cells were $ChAT^+$ indicating that they were indeed motoneurons. Data are means ± SD and analyzed using one-way ANOVAs for each property.

| **Motoneuron basal properties (N= 65 MNs, 40 animals (P0-P4))** | | | | | | | | | |
|---|---|---|---|---|---|---|---|---|---|
| **Property** | **$Chat^+$ filled MNs (8,5)[1]** | **Vehicle [2] (12,6)[2]** | **1 µM DA (7,4)[3]** | **5 µM DA (7,4)[4]** | **10 µM DA (6,5)[5]** | **100 µM DA (5,4)[6]** | **SKF 81297 (8,5)[7]** | **Quinpirole (12, 7)[8]** | **(7,56) F, p** |
| **Passive properties** | | | | | | | | | |
| Capacitance (pF) | 203±54 | 203±35 | 193±55 | 194.3±45 | 149±66 | 244±54 | 199±50 | 210±43 | 1.6, 0.15 |
| $V_m$ (mV) | -73±4.1 | -74±4.3 | -75±4.1 | -73±4.7 | -73±3.7 | -76±3.5 | -72±6.1 | -73±5.0 | 0.7, 0.7 |
| $I_{Holding\ -75mV}$ (pA) | -86±148 | -25±138 | 26±125 | -63±85 | 23±150 | -101±99 | -38±87 | -74±62 | 1.16, 0.3 |
| Rin (MΩ) | 50±15 | 48±24 | 59±44 | 70±83 | 115±84 | 40±9.2 | 71±28 | 49±14 | 2.0, 0.07 |
| Rheobase (pA) | 678±225 | 747±386 | 596±367 | 464±286 | 443±390 | 762±318 | 580±298 | 633±260 | 0.9, 0.5 |
| **Spike Properties** | | | | | | | | | |
| $AP_{TH}$ (mV) | -51±4.4 | -55±4.4 | -55±4.2 | -52±5.9 | -56±3.5 | -53±2.5 | -54±4.3 | -55±4.4 | 1.0, 0.4 |
| $AP_{AMP}$ (mV) | 66±5.0 | 71±5.9 | 75±6.9 | 76±13 | 76±4.2 | 69±5.7 | 71±9.6 | 72±6.1 | 1.6, 0.2 |
| $AP_{rise\ time}$ (ms) | 0.45±0.2 | 0.33±0.1 | 0.37±0.1 | 0.4±0.1 | 0.44±0.1 | 0.32±0.04 | 0.35±0.05 | 0.33±0.1 | 1.6, 0.2 |
| $AP_{half\ width}$ (ms) | 0.59±0.15 | 0.60±0.1 | 0.64±0.2 | 0.78±0.3 | 0.75±0.2 | 0.62±0.07 | 0.68±0.1 | 0.68±0.19 | 1.2, 0.3 |
| $AHP_{duration}$ (ms) | 73.7±29 | 70±18 | 88±34 | 76±13 | 108±38 | 74±16 | 69±23 | 76±26 | 1.5, 0.2 |
| $AHP_{AMP}$ (mV) | -3.9±1.1 | 3.6±2.2 | 3.1±1.4 | 3.2±1.4 | 3.4±2.1 | 4.7±1.2 | -4.2±1.9 | -4.3±1.4 | 0.8, 0.6 |
| **Repetitive Firing Properties** | | | | | | | | | |
| SS F/I Slope (Hz/pA) | 0.053±0.01 | 0.044±0.008 | 0.058±0.008 | 0.052±0.018 | 0.053±0.03 | 0.051±0.007 | 0.046±0.008 | 0.053±0.012 | 1.2, 0.3 |
| Repetitive firing TH (pA) | 605±446 | 498±254 | 410±271 | 354±200 | 338±327 | 515±253 | 367±186 | 494±173 | 0.8, 0.6 |
| Max SS firing rate (Hz) | 59±8.1 | 59±8.3 | 51±13 | 46±7.9 | 52±8.9 | 55±12 | 57±9.5 | 58±12 | 1.9, 0.09 |
| First spike latency (ms) | 146±86 | 116±57 | 124±77 | 91±34 | 113±79 | 136±55 | 132±67 | 142±50 | 0.5, 0.8 |

***Table 2: Baseline ventral interneuron intrinsic properties***

Passive, spike, and repetitive firing properties of ventral interneurons that responded to quinpirole with sustained hyperpolarization of membrane potential (responders) were compared with those that did not respond (non-responders) and also retrogradely labelled descending commissural interneurons (dCINs). Responders had higher capacitance and holding current than non - responders and dCINs. Data are means ± SD; F and p values are reported from one-way ANOVAs for each property. Red values highlight variables where significant main effects were detected with $p < 0.05$. Superscript numbers reflect significant differences between respective conditions from post hoc analysis.

| **Ventral Interneurons (n=40 cells, 22 animals (P0-4))** | | | | |
|---|---|---|---|---|
| **Property** | **Non-responders[1] (n=20,8)** | **Responders[2] (n=10,9)** | **dCINs[3] (n=10,5)** | **(2,37) F, p** |
| **Passive Properties** | | | | |
| Capacitance (pF) | 47±15[2] | 73±40[1] | 46±17[2] | 4.2, 0.02 |
| $V_m$ (mV) | -66±4.3 | -66±5.2 | -66±6.0 | 0.02, 0.98 |
| $I_{Holding\ -75mV}$ (pA) | -10.8±16[2] | -57±52[1] | -26±18 | 4.9, 0.02 |
| Rin (MΩ) | 759±466 | 497±248 | 719±326 | 1.6, 0.1 |
| Rheobase (pA) | 84±103 | 59±13 | 47±13 | 0.9, 0.4 |
| **Spike Properties** | | | | |
| $AP_{TH}$ (mV) | -55±4.6 | -55±2.9 | -56±2.3 | 0.2, 0.8 |
| $AP_{AMP}$ (mV) | 71±9.3 | 71±8.2 | 72±7.3 | 0.05, 0.95 |
| $AP_{rise\ time}$ (ms) | 0.99±0.48[3] | 0.92±0.3[3] | 1.4±0.25[1,2] | 4.2, 0.023 |
| $AP_{half\ width}$ (ms) | 1.2±0.5 | 1.4±0.6[3] | 1.9±0.4[2] | 6.2, 0.005 |
| $AHP_{duration}$ (ms) | 173±96 | 193±76 | 172±81 | 0.2, 0.8 |
| $AHP_{AMP}$ (mV) | -4.9±2.7 | -4.8±2.1 | -4.8±2.7 | 0.02, 0.98 |
| **Repetitive Firing Properties** | | | | |
| SS F/I slope (Hz/pA) | 0.24±0.07 | 0.21±0.09 | 0.2±0.1 | 1.0, 0.4 |
| Repetitive firing TH (pA) | 26±14 | 31±12 | 28±13 | 0.5, 0.6 |
| Max firing rate (Hz) | 43±16.3 | 39±11.6 | 32±5.9 | 2.1, 0.13 |
| Fist spike latency (ms) | 143±81 | 146±95 | 117±87 | 0.45, 0.6 |

## Figures and Captions

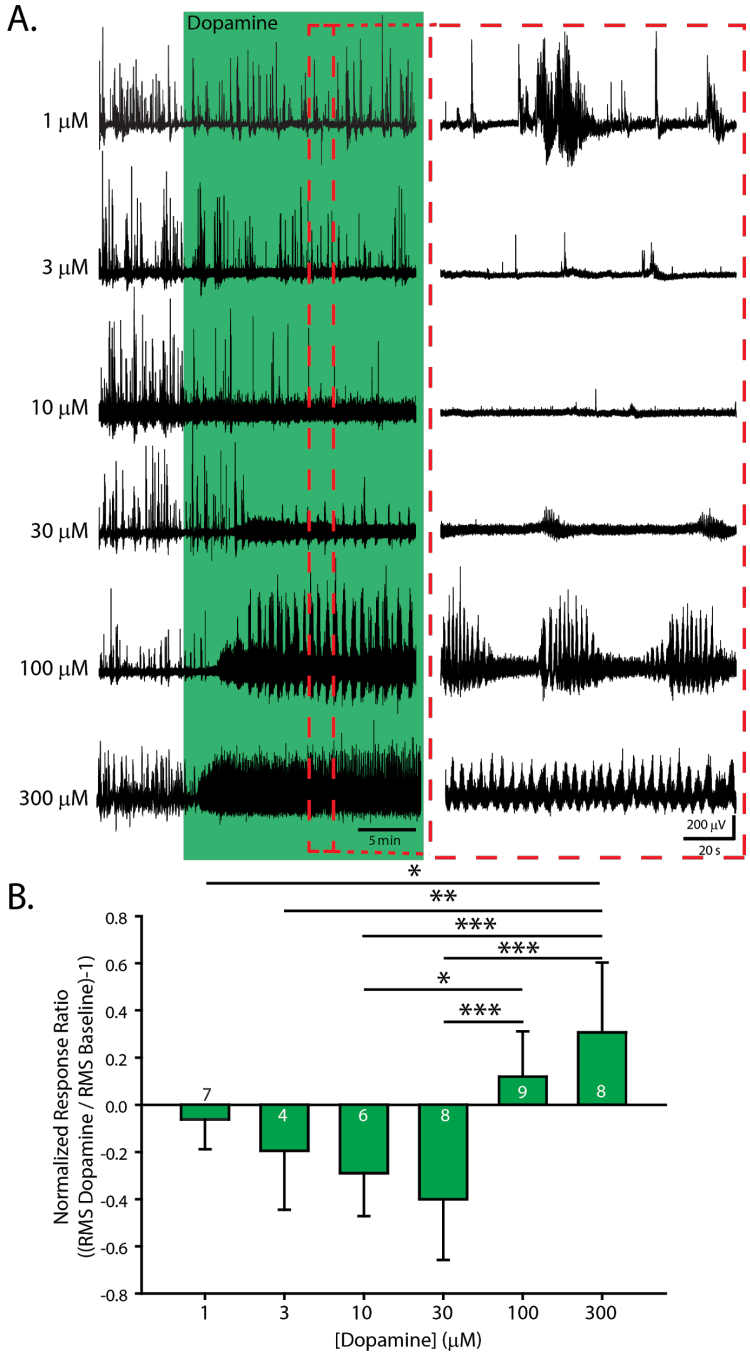


***Figure 1: Dopamine evokes bidirectional dose-dependent modulation of lumbar network activity***
A. Extracellular neurograms recorded from naïve single lumbar ventral root preparations after applying dopamine in various concentrations. Each row indicates a separate trial. Each recording began with spontaneous motor activity; the green section shows the effect of dopamine for each dose. The red-dashed box highlights expanded sections of data to the right of each neurogram. B. Mean normalized response ratios calculated from the root mean square of the raw neurogram during a 5-minute window, 20 minutes after dopamine application, compared to baseline activity. The negative response ratios represent inhibition and positive values represent excitation. The number in each green bar indicates the number of preparations in the average for each concentration. Error bars indicate standard deviation. Asterisks denote the significance level of Tukey post hoc tests between ratio concentrations (*$p < 0.05$, **$p < 0.01$, ***$p < 0.001$).

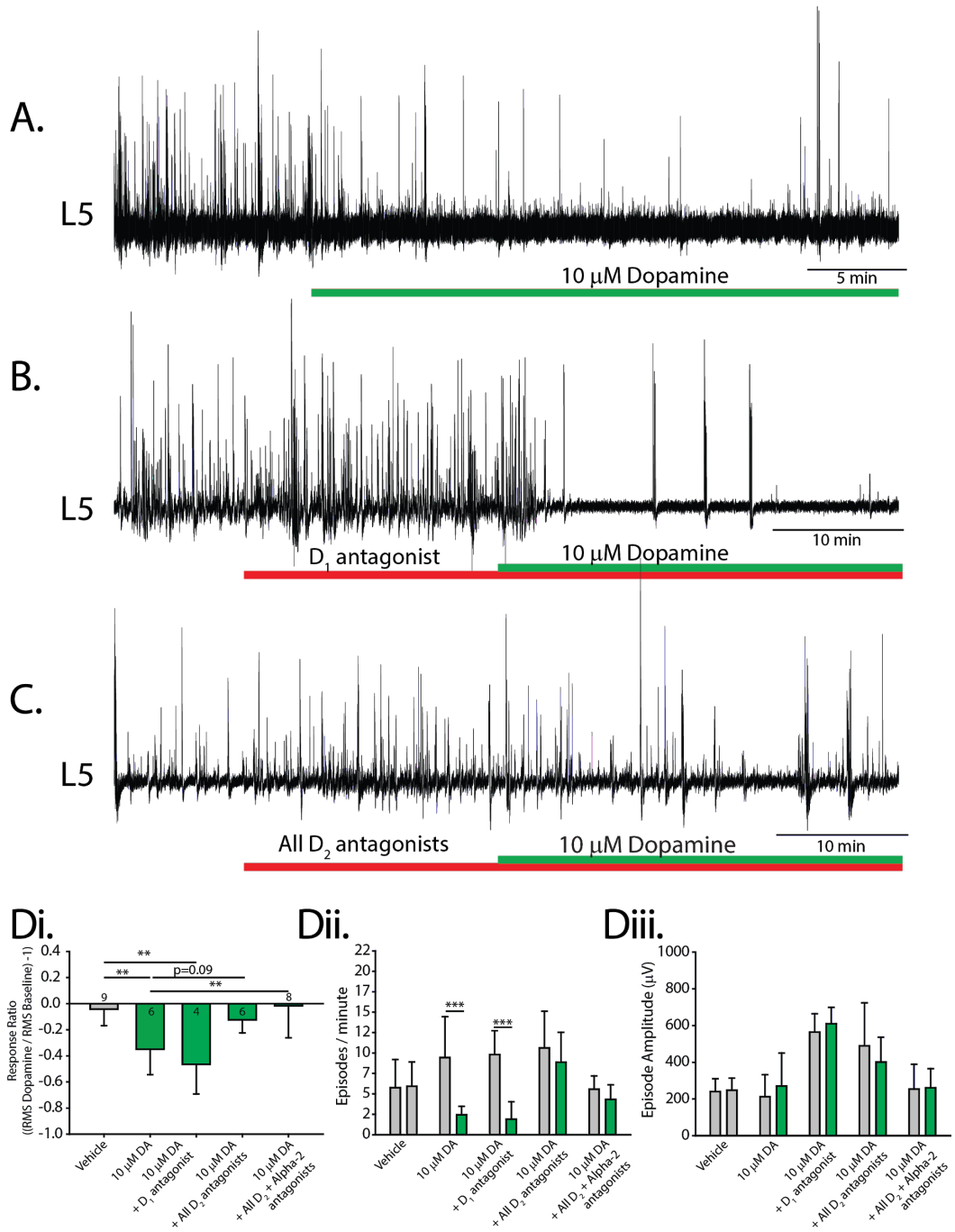


***Figure 2: Receptor mechanisms for dopaminergic inhibition of spontaneous network activity.***
A–C. Single ventral root (L5) extracellular neurograms of spontaneous activity in the presence of dopamine (A), a $D_1$ antagonist and dopamine (B), and with a cocktail of $D_2$ antagonists and dopamine (C). Spinal cords were perfused with receptor-preferring antagonists (red bars) 20 minutes prior to the application of low concentrations of dopamine (10 μM). D. Response ratio represents the root mean square of raw neurograms during a 5-minute window, 20 minutes after dopamine application, compared with prior to dopamine application. Negative response ratios indicate inhibition and positive values indicate excitation. The number in each bar indicates the number of preparations included in that condition's mean. Bars indicate the mean (± SD), number of episodes per minute (Dii), and amplitude (Diii) of spontaneous episodes recorded within the 5-minute epochs during which response ratios were calculated. Asterisks indicate the significance level of post hoc comparisons (*$p < 0.05$, **$p < 0.01$, ***$p < 0.001$).

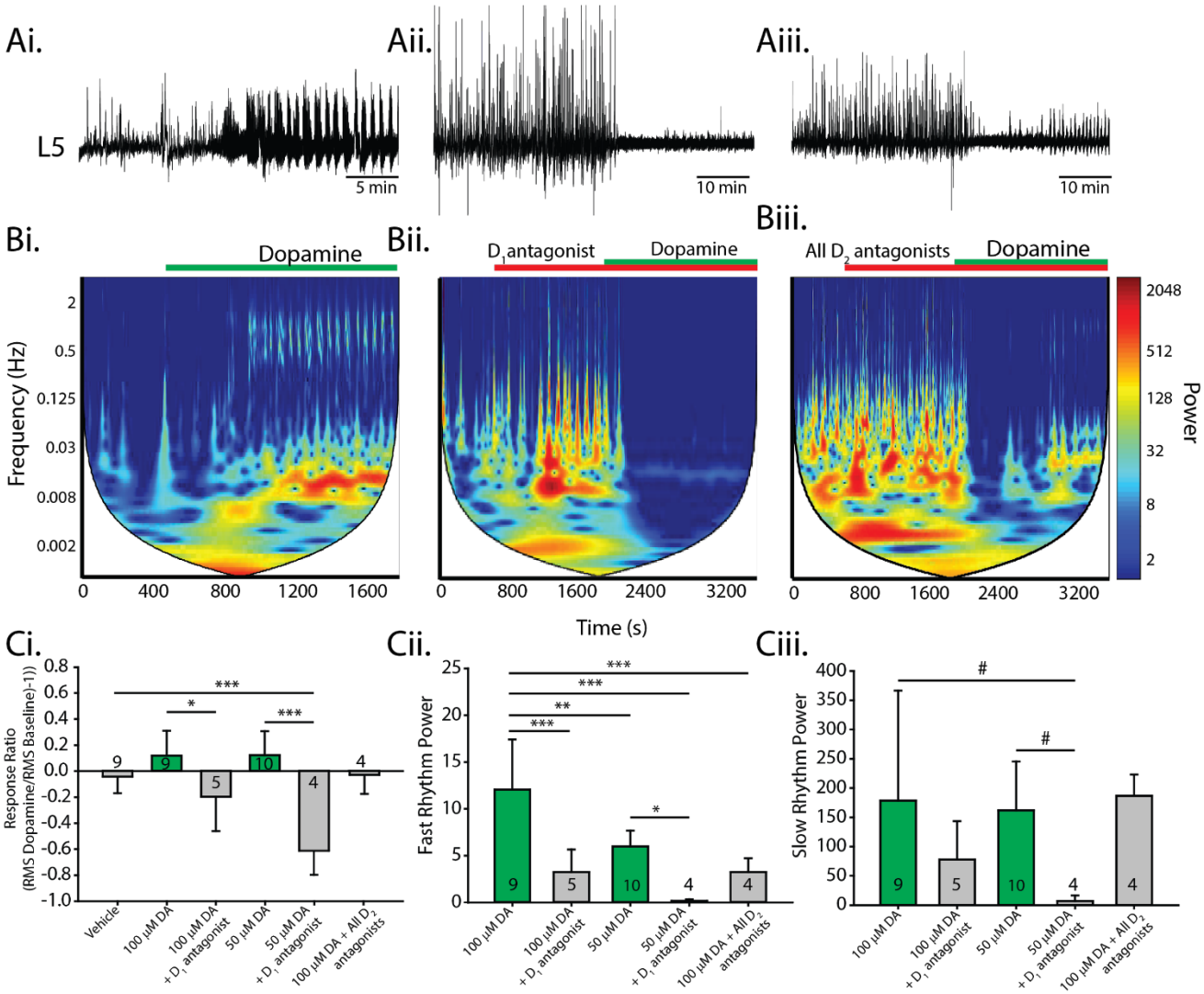


***Figure 3: Receptor mechanisms for dopaminergic excitation of spinal network activity.***
High concentrations of dopamine excite spinal networks and produce episodic and continuous rhythmic patterns of activity. A. Single ventral root extracellular neurograms of spinal network activity from each condition: dopamine applied alone (Ai), in the presence of a $D_1$ antagonist (Aii), and with a cocktail of $D_2$ antagonists (Aiii). Horizontal bars indicate the timing of dopamine application (green bars) and the application of receptor-preferring antagonists (red bars). B. Spectrograms show autowavelet frequency power across time, evoked at high concentrations of dopamine (50 -100 µM). The colour bar indicates power magnitude, from high (warm) to low (cool colours). We selected regions of interest around regions that coincided with fast and slow rhythm frequency rhythms. Spinal cords were perfused with antagonists for 20 minutes prior to the application of dopamine. Ci. Mean response ratios (± SD), as in Fig. 2, for each condition. Spectral analysis of fast rhythm (Cii) and slow rhythm (Ciii) power following drug application for each experimental condition. Histograms present mean values ± SD, with asterisks denoting significance level of post hoc tests (*$p < 0.05$, **$p < 0.01$, ***$p < 0.001$) following one-way ANOVA (fast rhythm; Cii) or nonparametric one-way ANOVA (slow rhythm; Ciii).

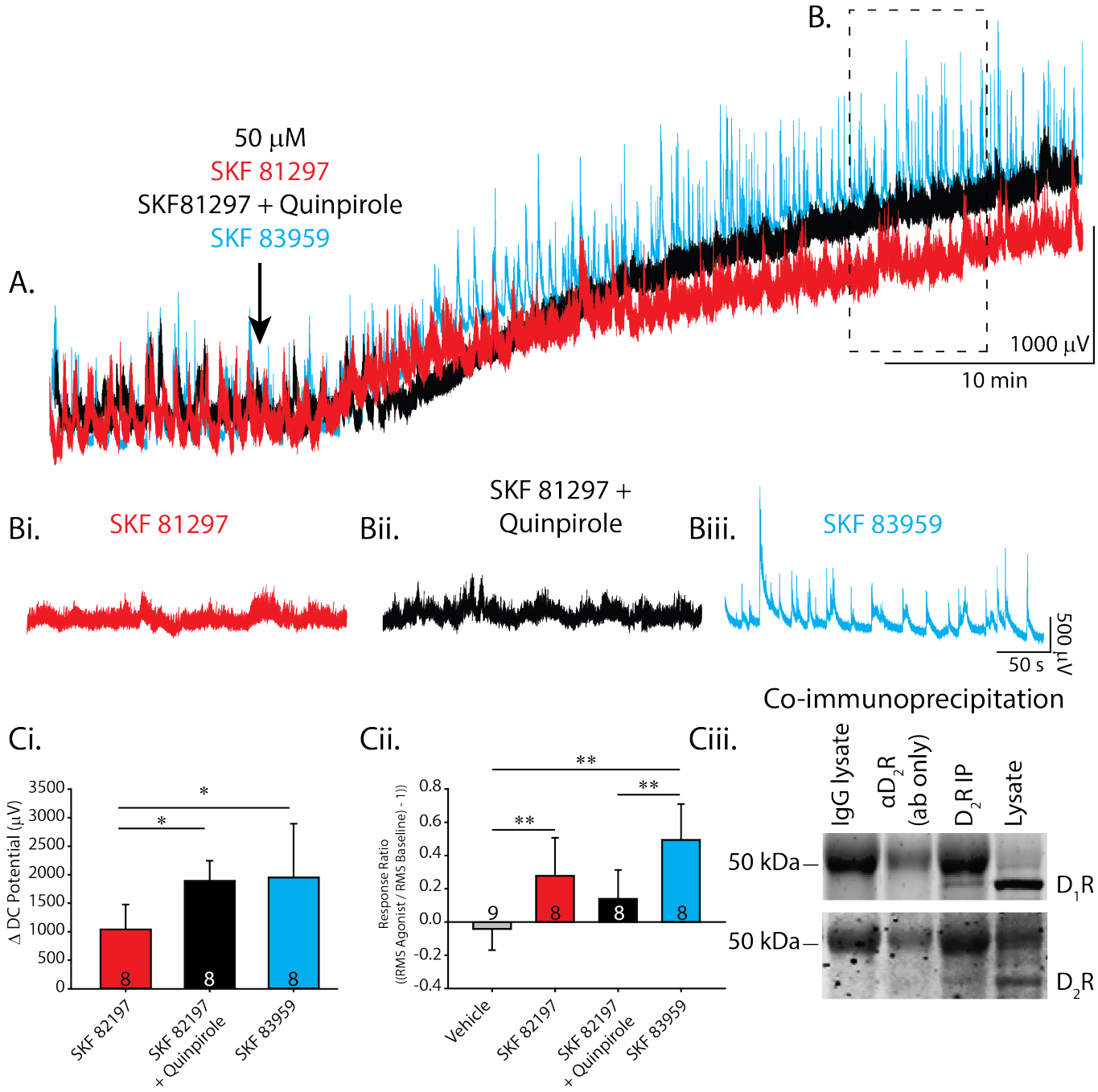


***Figure 4: $D_1$ $D_2$ receptor co-activation contributes to the excitatory effect of dopamine.***
A. Single ventral root extracellular DC neurograms of spontaneous activity from conditions where a $D_1$ agonist (SKF 81297) was applied alone (red), co-applied with a $D_2$ agonist (SKF 81297 + Quinpirole; black), or $D_1$ and $D_2$ receptors were coactivated by a $D_1/D_2$ co-agonist (SKF 83959; blue). Bi-iii. For each agonist, (B) expands the region of spontaneous activity 20–25 minutes after agonist application, as outlined by the dashed line in (A). C. Ci depicts depolarization of DC potentials from DC neurograms, averaged across the number of preparations denoted by numbers in each condition's bar. Cii shows the response ratio for each condition (as in previous figures), which represents changes in the amount of spontaneous activity. Ciii. Co-immunoprecipitation of $D_1$ with $D_2$ receptors suggests that they may interact in the neonatal spinal cord. Histograms present mean values ± SD, with asterisks denoting significance level of post hoc comparisons (*$p < 0.05$, **$p < 0.01$, ***$p < 0.001$) following one-way ANOVA.

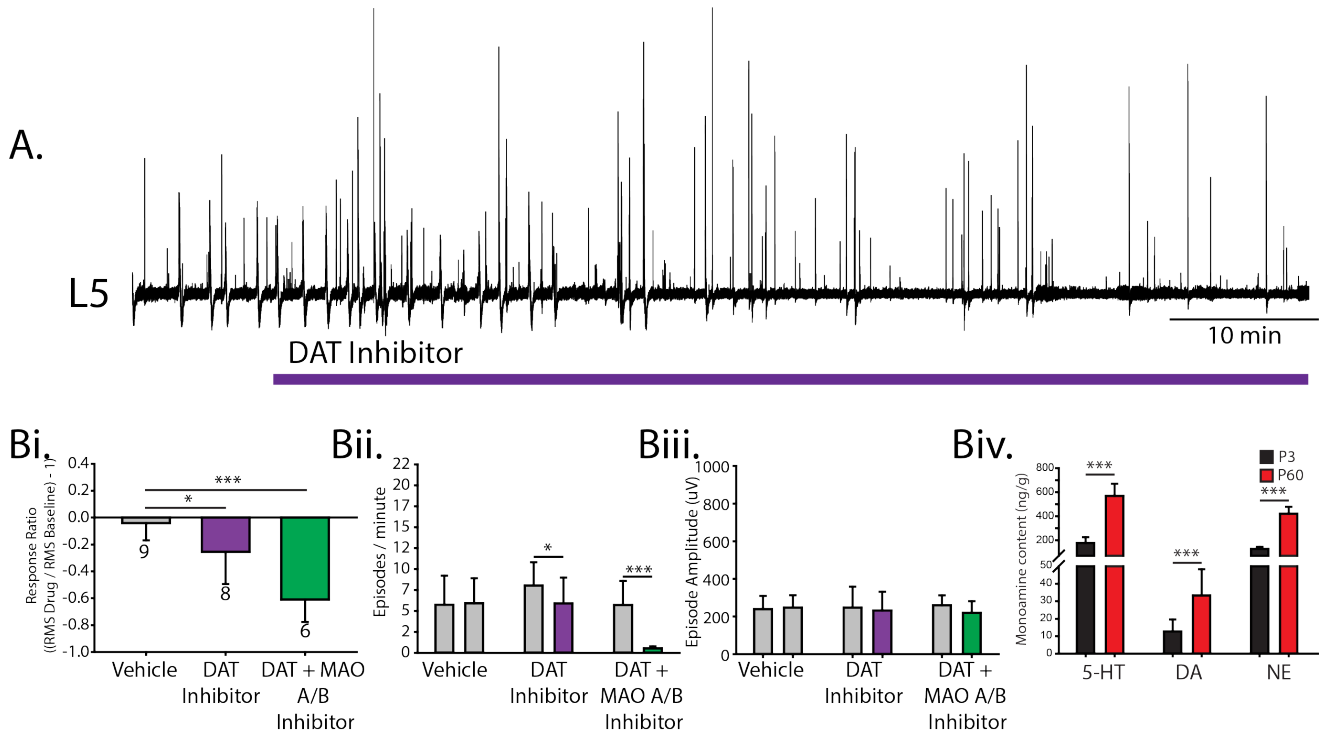


***Figure 5: Inhibitory actions of endogenous dopamine in the neonatal mouse spinal cord.***
A. Single ventral root (L5) neurogram of spontaneous activity after blocking the dopamine transporter (DAT) with the DAT antagonist GBR 12909 (purple) to increase the endogenous dopamine level. Dopamine reuptake was also blocked in the presence of monoamine oxidase A & B inhibitor bifemelane (green) to reduce dopamine metabolism. Bi illustrates the response ratio; negative and positive values indicate inhibition and excitation, respectively. The number below each bar represents the number of preparations for each experiment. Spontaneous episode occurrences per minute (Bii) and amplitude (Biii) were measured within the epochs where the response ratio was calculated. Histograms present mean values ± SD and asterisks indicate a significance level of post hoc analyses (*$p < 0.05$, **$p < 0.01$, ***$p < 0.001$) following one-way ANOVA for response ratios, and two-way ANOVA for burst occurrences and amplitude that compared between conditions. Biv. Endogenous levels of serotonin (5-HT), dopamine (DA) and norepinephrine (NE) were measured in neonatal (P3) and adult (P60) lumbar spinal cords with high-performance liquid chromatography.

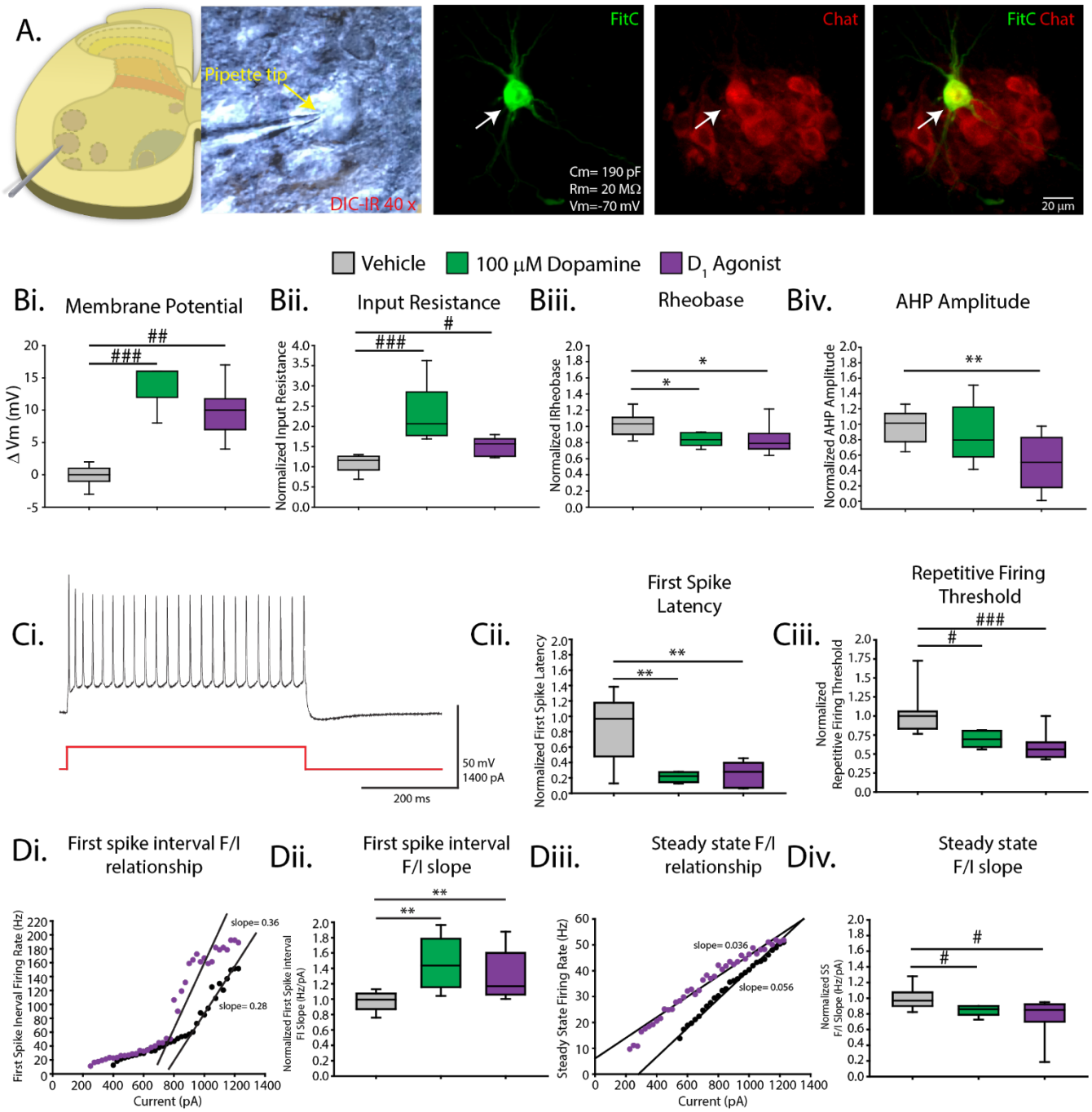


***Figure 6: High concentrations of dopamine and $D_1$ agonists increase motoneuron excitability***

A. Whole-cell patch-clamp recordings were obtained from motoneurons visualized with infrared differential interference contrast (IR-DIC) in lumbar slices of neonatal (P0–P4) mice. A subset of cells were filled with fluorescein (FITC, green) and verified post hoc with immunohistochemistry for choline acetyltransferase (ChAT, red). B–D. High concentrations of dopamine (100 µM, green) and the $D_1$ agonist SKF 81297 (20 µM, purple) increased motoneuron excitability by modulating various passive, spike, and repetitive firing properties. All measures were compared to that of time-matched vehicle control (grey). Ci. A typical motoneuron trace following current injection. Di, Diii display representative frequency–current (FI) plots from a single cell before (black dots) and after (purple dots) application of the $D_1$ agonist. Box and whisker plots display interquartile range (boxes), median (horizontal black lines), max, and minimum value in data range (whiskers). Asterisks denote significance level of post hoc tests (*$p < 0.05$, **$p < 0.01$, ***$p < 0.001$) following one-way ANOVA.

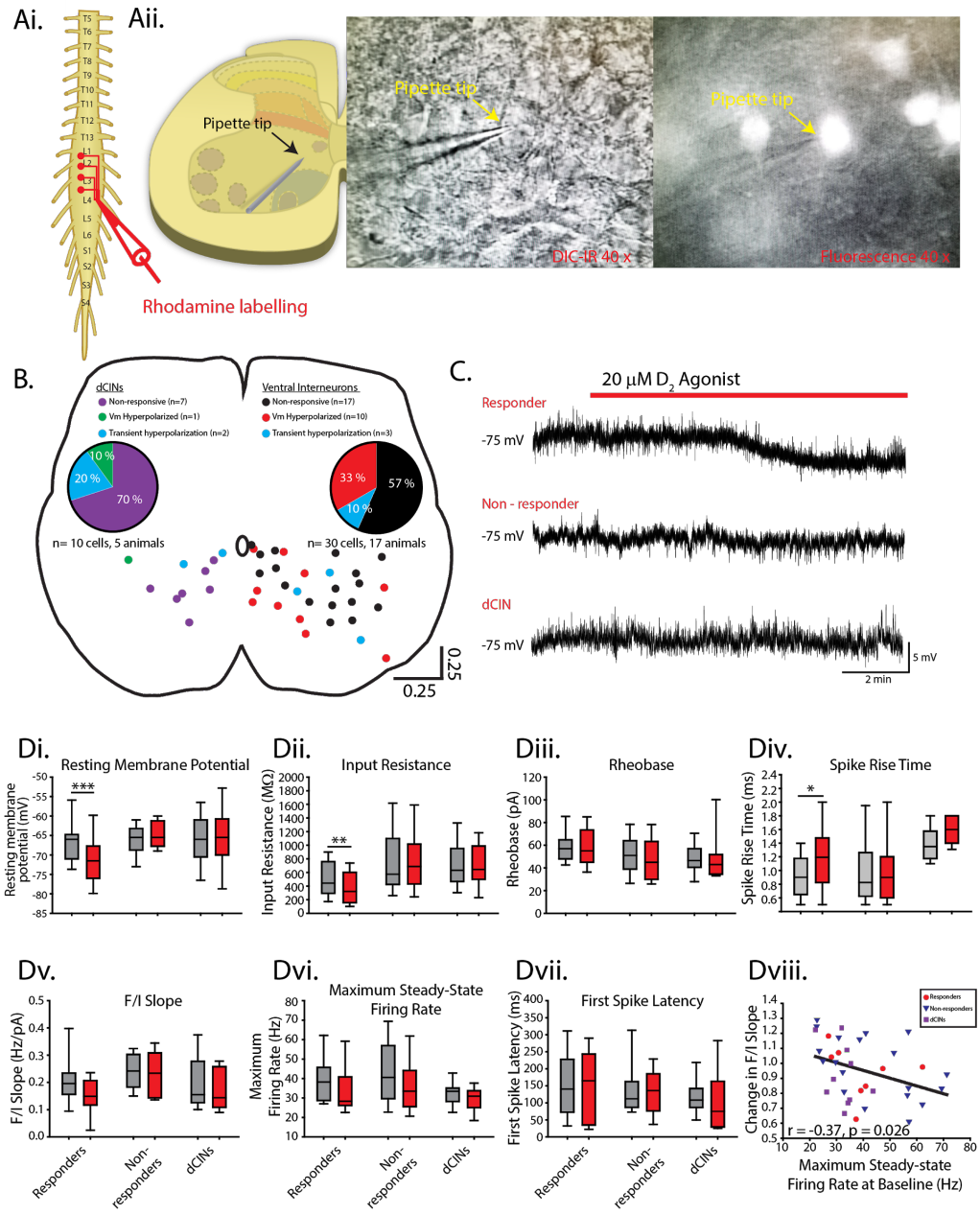


***Figure 7: $D_2$ agonists hyperpolarize a proportion of ventral interneurons.***
Whole-cell recordings obtained from lamina VII–X interneurons. Ai. Descending commissural interneurons (dCINs) were retrogradely labelled with rhodamine-conjugated dextran amine crystals inserted into the ventrolateral funiculus at L4 level. Aii. Cells were visualized in transverse lumbar slices under infrared differential interference contrast (IR-DIC) or epifluorescent illumination. B. Ventral interneuron location was measured relative to the central canal and X-Y positions normalized to the distance of ventral and lateral borders of lumbar slices. C. Whole-cell current-clamp recordings depict responsiveness of interneuron resting membrane potential to the $D_2$ agonist (quinpirole, 20 μM) in responders, non - responders, and dCINs. A proportion of ventral interneurons responded to quinpirole with either a sustained (B, red and green dots) or transient (B, blue dots) hyperpolarization of the membrane potential. A reduction in input resistance and increase in spike rise time accompanied hyperpolarization in sustained responders (Dii, Div). Box and whisker plots display interquartile range (boxes), median (horizontal black lines), max, and minimum value in data range (whiskers). asterisks denote significance level from post hoc tests (*$p < 0.05$, **$p < 0.01$, ***$p < 0.001$) following two-way ANOVA. Dviii. Reductions in steady-state frequency-current (FI) slope of all cells following application of quinpirole was greatest in cells that had a higher maximum steady-state firing rate at baseline.

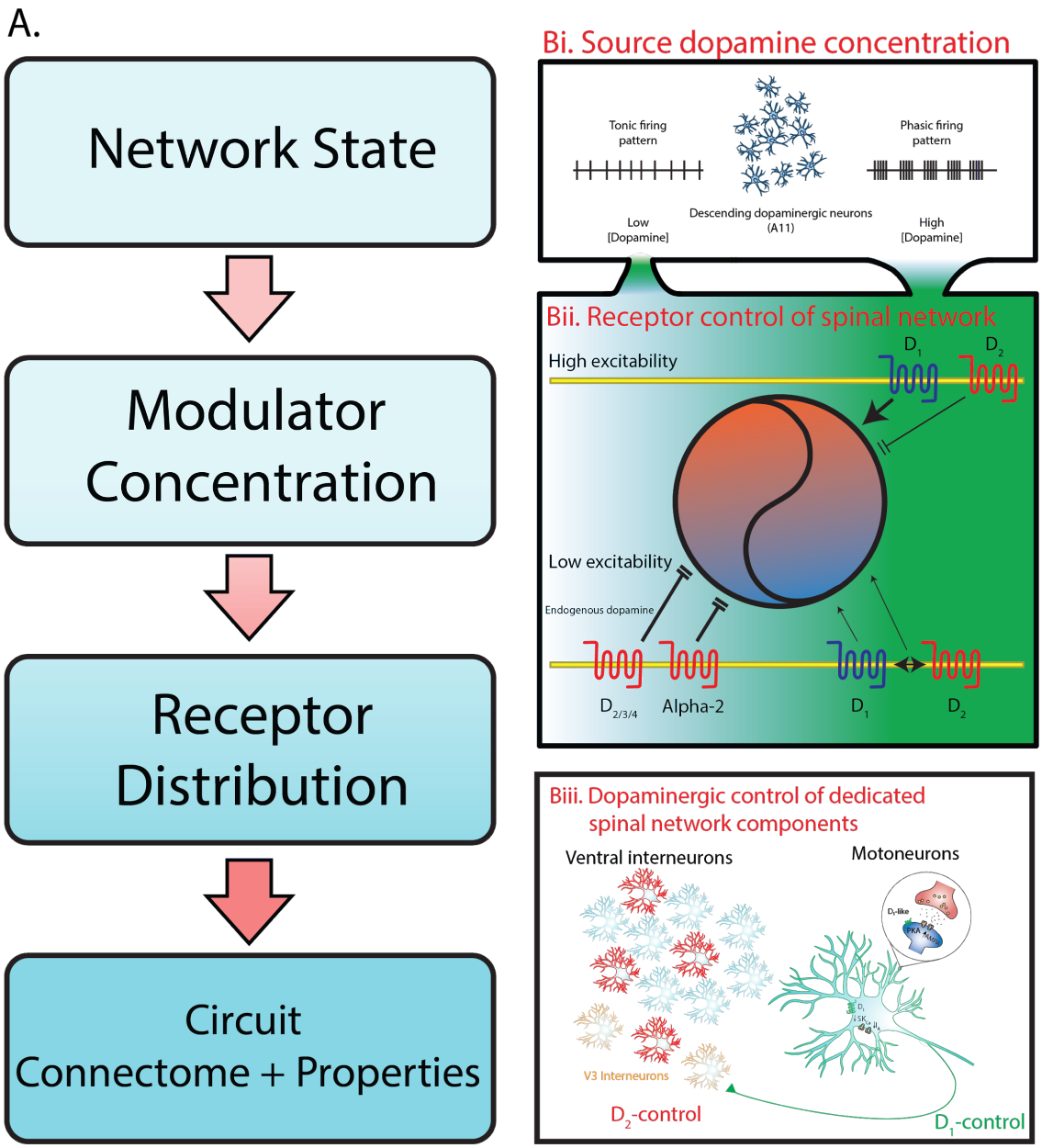


***Figure 8: Dopamine exerts state and receptor-dependent control of spinal motor networks.***
A. Neural network output is dependent on multiple factors. Circuit connectomes and intrinsic properties defining constraints of a network output. Similarly, the distribution of neuromodulator receptors defines the constraints on which neuromodulators can alter these properties. Varying ligand affinities of these receptors determine dose-dependent effect of neuromodulators and network state dictates the dose-dependent effects of neuromodulators. Bi. Previous work has demonstrated that tonic and phasic firing patterns of dopamine cells lead to the release of low and high concentrations of dopamine, respectively [10]. Bii. During a low excitability state (blue part of the circle), low concentrations of dopamine (denoted by the green gradient) acted on $D_2$, $D_3$, $D_4$ and α2-adrenergic receptors in parallel to inhibit (parallel stop lines) spinal motor output. As dopamine levels rise, activation of $D_1$ and co-activation of $D_2$ receptors increase (arrowheads) spinal network output. During a high excitability state (orange part of the circle), the actions of low dopamine are not apparent and at higher concentrations, activation of $D_1$ receptors boost spinal network output and activation of $D_2$ receptors slows rhythmic activity [13]. Biii. Higher concentrations of dopamine act through $D_1$ receptors to increase motoneuron excitability by reducing A-type and $SK_{Ca}$-dependent calcium conductance. $D_2$-mediated inhibition of spinal network output is triggered by reduced excitability in a proportion of ventral interneurons (red cells).

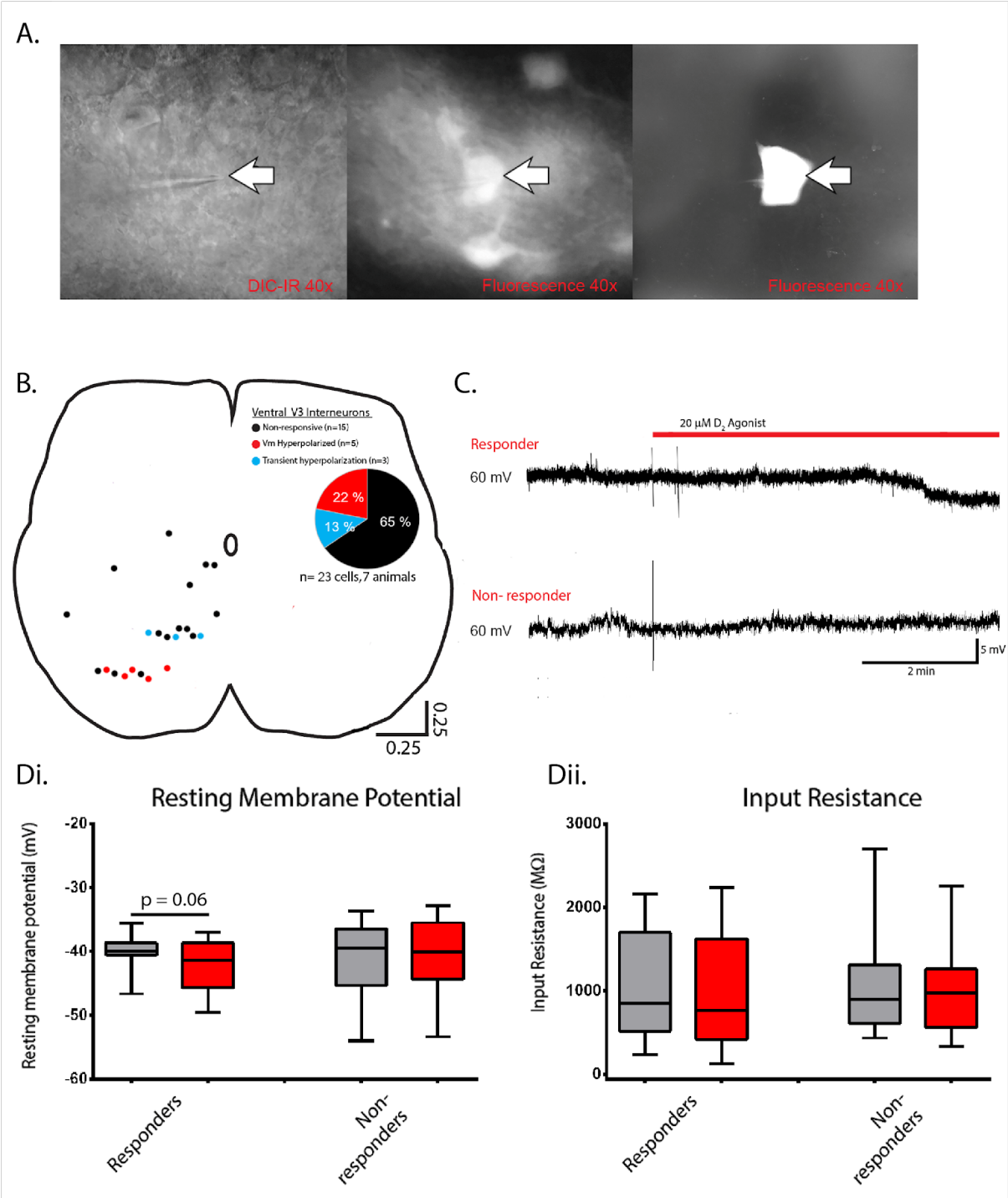


***Supplemental Figure 1*: $D_2$ - receptor control of V3 interneurons.**
Whole-cell patch-clamp recordings obtained from lamina V3 interneurons. A. Visually guided patch showing pipette tip on a GFP labelled-V3 interneuron. B. V3 interneuron location was measured relative to the central canal and X-Y positions normalized to the distance of ventral and lateral borders of lumbar slices. Non-responders represented by black dots, responders by red dots, and transient responders by blue dots. C. A sample trace showing a hyperpolarization of the resting membrane potential following administration of 20 µM quinpirole in responders (top trace) and non-responders (bottom trace). Di. Box and whisker plots showing a change in resting membrane potential in responders and non-responders before (gray) and after (red) administration of quinpirole. Dii. Input resistance graphed in a similar manner as Di.

**References**


1. Miles GB, Sillar KT. Neuromodulation of vertebrate locomotor control networks. Physiology. 2011;26: 393–411.

2. Marder E, Thirumalai V. Cellular, synaptic and network effects of neuromodulation. Neural Netw. 2002;15: 479–493.

3. Stein W. Modulation of stomatogastric rhythms. J Comp Physiol A Neuroethol Sens Neural Behav Physiol. 2009;195: 989–1009.

4. Grillner S, Robertson B. The Basal Ganglia Over 500 Million Years. Curr Biol. 2016;26: R1088–R1100.

5. Kravitz AV, Freeze BS, Parker PRL, Kay K, Thwin MT, Deisseroth K, et al. Regulation of parkinsonian motor behaviours by optogenetic control of basal ganglia circuitry. Nature. 2010;466: 622–626.

6. Bateup HS, Santini E, Shen W, Birnbaum S, Valjent E, Surmeier DJ, et al. Distinct subclasses of medium spiny neurons differentially regulate striatal motor behaviors [Internet]. Proceedings of the National Academy of Sciences. 2010. pp. 14845–14850. doi:10.1073/pnas.1009874107

7. Roseberry TK, Lee AM, Lalive AL, Wilbrecht L, Bonci A, Kreitzer AC. Cell-Type-Specific Control of Brainstem Locomotor Circuits by Basal Ganglia. Cell. 2016;164: 526–537.

8. Sharples SA, Koblinger K, Humphreys JM, Whelan PJ. Dopamine: a parallel pathway for the modulation of spinal locomotor networks. Front Neural Circuits. 2014;8: 55.

9. Jay M, De Faveri F, McDearmid JR. Firing dynamics and modulatory actions of supraspinal dopaminergic neurons during zebrafish locomotor behavior. Curr Biol. 2015;25: 435–444.

10. Dreyer JK, Herrik KF, Berg RW, Hounsgaard JD. Influence of phasic and tonic dopamine release on receptor activation. J Neurosci. 2010;30: 14273–14283.

11. Lambert AM. Dopaminergic Control of Locomotor Patterning during Development: A Tail for the Ages. Front Cell Neurosci. 2016;10: 95.

12. Clemens S, Belin-Rauscent A, Simmers J, Combes D. Opposing modulatory effects of D1- and D2-like receptor activation on a spinal central pattern generator. J Neurophysiol. 2012;107: 2250–2259.

13. Sharples SA, Whelan PJ. Modulation of Rhythmic Activity in Mammalian Spinal Networks Is Dependent on Excitability State. eNeuro. 2017;4. doi:10.1523/ENEURO.0368-16.2017

14. Marder E, O'Leary T, Shruti S. Neuromodulation of circuits with variable parameters: single neurons and small circuits reveal principles of state-dependent and robust neuromodulation. Annu Rev Neurosci. 2014;37: 329–346.

15. Gutierrez GJ, O'Leary T, Marder E. Multiple mechanisms switch an electrically coupled, synaptically inhibited neuron between competing rhythmic oscillators. Neuron. 2013;77: 845–858.

16. Bonnot A, Morin D, Viala D. Genesis of spontaneous rhythmic motor patterns in the lumbosacral spinal cord of neonate mouse. Brain Res Dev Brain Res. 1998;108: 89–99.

17. Dalrymple AN, Sharples SA, Osachoff N, Lognon AP, Whelan PJ. A supervised machine learning approach to characterize spinal network function. J Neurophysiol. 2019;121: 2001–2012.

18. Hanson MG, Landmesser LT. Normal patterns of spontaneous activity are required for correct motor axon guidance and the expression of specific guidance molecules. Neuron. 2004;43: 687–701.

19. Ren J, Greer JJ. Ontogeny of rhythmic motor patterns generated in the embryonic rat spinal cord. J Neurophysiol. 2003;89: 1187–1195.

20. Whelan P, Bonnot A, O'Donovan MJ. Properties of rhythmic activity generated by the isolated spinal cord of the neonatal mouse. J Neurophysiol. 2000;84: 2821–2833.

21. Barriere G, Mellen N, Cazalets J-R. Neuromodulation of the locomotor network by dopamine in the isolated spinal cord of newborn rat. Eur J Neurosci. 2004;19: 1325–1335.

22. Lapointe NP, Rouleau P, Ung R-V, Guertin PA. Specific role of dopamine D1 receptors in spinal network activation and rhythmic movement induction in vertebrates. J Physiol. 2009;587: 1499–1511.

23. Sharples SA, Humphreys JM, Jensen AM, Dhoopar S, Delaloye N, Clemens S, et al. Dopaminergic modulation of locomotor network activity in the neonatal mouse spinal cord. J Neurophysiol. 2015;113: 2500–2510.

24. Picton LD, Nascimento F, Broadhead MJ, Sillar KT, Miles GB. Sodium Pumps Mediate Activity-Dependent Changes in Mammalian Motor Networks. J Neurosci. 2017;37: 906–921.

25. Acton D, Broadhead MJ, Miles GB. Modulation of spinal motor networks by astrocyte-derived adenosine is dependent on D-like dopamine receptor signaling. J Neurophysiol. 2018;120: 998–1009.

26. Mandadi S, Leduc-Pessah H, Hong P, Ejdrygiewicz J, Sharples SA, Trang T, et al. Modulatory and plastic effects of kinins on spinal cord networks. J Physiol. 2016;594: 1017–1036.

27. Gozal EA, O'Neill BE, Sawchuk MA, Zhu H, Halder M, Chou C-C, et al. Anatomical and functional evidence for trace amines as unique modulators of locomotor function in the mammalian spinal cord. Front Neural Circuits. 2014;8: 134.

28. Milan L, Barrière G, De Deurwaerdère P, Cazalets J-R, Bertrand SS. Monoaminergic control of spinal locomotor networks in SOD1G93A newborn mice. Front Neural Circuits. 2014;8: 77.

29. Madriaga MA, McPhee LC, Chersa T, Christie KJ, Whelan PJ. Modulation of locomotor activity by multiple 5-HT and dopaminergic receptor subtypes in the neonatal mouse spinal cord. J Neurophysiol. 2004;92: 1566–1576.

30. Gordon IT, Whelan PJ. Monoaminergic control of cauda-equina-evoked locomotion in the neonatal mouse spinal cord. J Neurophysiol. 2006;96: 3122–3129.

31. Humphreys JM, Whelan PJ. Dopamine exerts activation-dependent modulation of spinal locomotor circuits in the neonatal mouse. J Neurophysiol. 2012;108: 3370–3381.

32. Chopek JW, Nascimento F, Beato M, Brownstone RM, Zhang Y. Sub-populations of Spinal V3 Interneurons Form Focal Modules of Layered Pre-motor Microcircuits. Cell Rep. 2018;25: 146–156.e3.

33. Simon A Sharples, Nicole E Burma, Heather Leduc-Pessah, Celine Jean-Xavier and Patrick J Whelan. Complex dopamine receptor interactions exert diverse modulation on spinal networks of the neonatal mouse. 2017. doi: 10.13140/RG.2.2.17191.09125

34. Simon A. Sharples and Patrick J. Whelan. Dopamine exerts concentration-dependent bidirectional modulation and evoked state-dependent NMDA-mediated rhythmicity in motor networks of the neonatal mouse spinal cord. 2015. doi:10.13140/RG.2.2.31925.27368

35. LaHoste GJ, Marshall JF. The role of dopamine in the maintenance and breakdown of D1/D2 synergism. Brain Res. 1993;611: 108–116.

36. Lee SP, So CH, Rashid AJ, Varghese G, Cheng R, José Lança A, et al. Dopamine D1 and D2 Receptor Co-activation Generates a Novel Phospholipase C-mediated Calcium Signal. J Biol Chem. 2004;279: 35671–35678.

37. Rashid AJ, So CH, Kong MMC, Furtak T, El-Ghundi M, Cheng R, et al. D1-D2 dopamine receptor heterooligomers with unique pharmacology are coupled to rapid activation of Gq/11 in the striatum. Proc Natl Acad Sci U S A. 2007;104: 654–659.

38. Thompson JL, Yang J, Lau B, Liu S, Baimel C, Kerr LE, et al. Age-Dependent D1-D2 Receptor Coactivation in the Lateral Orbitofrontal Cortex Potentiates NMDA Receptors and Facilitates Cognitive Flexibility. Cereb Cortex. 2016;26: 4524–4539.

39. Rashid AJ, So CS, O'Dowd BF, George SR. S.19.05 Heterooligomerization of D1 and D2 dopamine receptors in brain: implications for psychosis? Eur Neuropsychopharmacol. 2006;16: S193.

40. Falgairolle M, Puhl JG, Pujala A, Liu W, O'Donovan MJ. Motoneurons regulate the central pattern generator during drug-induced locomotor-like activity in the neonatal mouse [Internet]. eLife. 2017. doi:10.7554/elife.26622

41. Button DC, Kalmar JM, Gardiner K, Cahill F, Gardiner PF. Spike frequency adaptation of rat hindlimb motoneurons. J Appl Physiol. 2007;102: 1041–1050.

42. Bos R, Harris-Warrick RM, Brocard C, Demianenko LE, Manuel M, Zytnicki D, et al. Kv1.2 Channels Promote Nonlinear Spiking Motoneurons for Powering Up Locomotion. Cell Rep. 2018;22: 3315–3327.

43. Miles GB, Dai Y, Brownstone RM. Mechanisms underlying the early phase of spike frequency adaptation in mouse spinal motoneurones. J Physiol. 2005;566: 519–532.

44. Han P, Nakanishi ST, Tran MA, Whelan PJ. Dopaminergic modulation of spinal neuronal excitability. J Neurosci. 2007;27: 13192–13204.

45. Han P, Whelan PJ. Modulation of AMPA currents by D(1)-like but not D(2)-like receptors in spinal motoneurons. Neuroscience. 2009;158: 1699–1707.

46. Quinlan KA, Kiehn O. Segmental, synaptic actions of commissural interneurons in the mouse spinal cord. J Neurosci. 2007;27: 6521–6530.

47. Butt SJB, Kiehn O. Functional identification of interneurons responsible for left-right coordination of hindlimbs in mammals. Neuron. 2003;38: 953–963.

48. Kiehn O, Butt SJB. Physiological, anatomical and genetic identification of CPG neurons in the

developing mammalian spinal cord. Prog Neurobiol. 2003;70: 347–361.

49. Abbinanti MD, Zhong G, Harris-Warrick RM. Postnatal emergence of serotonin-induced plateau potentials in commissural interneurons of the mouse spinal cord. J Neurophysiol. 2012;108: 2191–2202.

50. Zhong G, Díaz-Ríos M, Harris-Warrick RM. Intrinsic and functional differences among commissural interneurons during fictive locomotion and serotonergic modulation in the neonatal mouse. J Neurosci. 2006;26: 6509–6517.

51. Restrepo CE, Lundfald L, Szabó G, Erdélyi F, Zeilhofer HU, Glover JC, et al. Transmitter-phenotypes of commissural interneurons in the lumbar spinal cord of newborn mice. J Comp Neurol. 2009;517: 177–192.

52. Butt SJB, Harris-Warrick RM, Kiehn O. Firing properties of identified interneuron populations in the mammalian hindlimb central pattern generator. J Neurosci. 2002;22: 9961–9971.

53. Zhang Y, Narayan S, Geiman E, Lanuza GM, Velasquez T, Shanks B, et al. V3 spinal neurons establish a robust and balanced locomotor rhythm during walking. Neuron. 2008;60: 84–96.

54. Borowska J, Jones CT, Zhang H, Blacklaws J, Goulding M, Zhang Y. Functional subpopulations of V3 interneurons in the mature mouse spinal cord. J Neurosci. 2013;33: 18553–18565.

55. Borowska J, Jones CT, Deska-Gauthier D, Zhang Y. V3 interneuron subpopulations in the mouse spinal cord undergo distinctive postnatal maturation processes. Neuroscience. 2015;295: 221–228.

56. Falgairolle M, O'Donovan MJ. Feedback regulation of locomotion by motoneurons in the vertebrate spinal cord [Internet]. Current Opinion in Physiology. 2019. pp. 50–55. doi:10.1016/j.cophys.2018.12.009

57. Grillner S, Robertson B, Stephenson-Jones M. The evolutionary origin of the vertebrate basal ganglia and its role in action selection. J Physiol. 2013;591: 5425–5431.

58. Picton LD, Sillar KT. Mechanisms underlying the endogenous dopaminergic inhibition of spinal locomotor circuit function in Xenopus tadpoles. Sci Rep. 2016;6: 35749.

59. Murray KC, Nakae A, Stephens MJ, Rank M, D'Amico J, Harvey PJ, et al. Recovery of motoneuron and locomotor function after spinal cord injury depends on constitutive activity in 5-HT2C receptors. Nat Med. Nature Publishing Group; 2010;16: 694–700.

60. Meng D, Li H-Q, Deisseroth K, Leutgeb S, Spitzer NC. Neuronal activity regulates neurotransmitter switching in the adult brain following light-induced stress. Proc Natl Acad Sci U S A. 2018;115: 5064–5071.

61. Ben-Ari Y, Khazipov R, Leinekugel X, Caillard O, Gaiarsa JL. GABAA, NMDA and AMPA receptors: a developmentally regulated "ménage à trois." Trends Neurosci. 1997;20: 523–529.

62. Allene C, Cossart R. Early NMDA receptor-driven waves of activity in the developing neocortex: physiological or pathological network oscillations? J Physiol. 2010;588: 83–91.

63. Koblinger K, Jean-Xavier C, Sharma S, Füzesi T, Young L, Eaton SEA, et al. Optogenetic Activation of A11 Region Increases Motor Activity. Front Neural Circuits. 2018;12: 86.

64. Musienko P, van den Brand R, Märzendorfer O, Roy RR, Gerasimenko Y, Edgerton VR, et al. Controlling specific locomotor behaviors through multidimensional monoaminergic modulation of spinal circuitries. J Neurosci. 2011;31: 9264–9278.

65. Bolton AD, Murata Y, Kirchner R, Kim S-Y, Young A, Dang T, et al. A Diencephalic Dopamine Source Provides Input to the Superior Colliculus, where D1 and D2 Receptors Segregate to Distinct Functional Zones. Cell Rep. 2015;13: 1003–1015.

66. Rotstein HG, Schneider E, Szczupak L. Feedback Signal from Motoneurons Influences a Rhythmic Pattern Generator. J Neurosci. 2017;37: 9149–9159.

67. Matsunaga T, Kohsaka H, Nose A. Gap Junction-Mediated Signaling from Motor Neurons Regulates Motor Generation in the Central Circuits of Larval. J Neurosci. 2017;37: 2045–2060.

68. Marder E, Bucher D. Central pattern generators and the control of rhythmic movements. Curr Biol. 2001;11: R986–96.

69. Song J, Ampatzis K, Rebecka Björnfors E, El Manira A. Motor neurons control locomotor circuit function retrogradely via gap junctions [Internet]. Nature. 2016. pp. 399–402. doi:10.1038/nature16497

70. Pujala A, Blivis D, O'Donovan MJ. Interactions between Dorsal and Ventral Root Stimulation on the Generation of Locomotor-Like Activity in the Neonatal Mouse Spinal Cord [Internet]. eneuro. 2016. pp. ENEURO.0101–16.2016. doi:10.1523/eneuro.0101-16.2016

71. Bhumbra GS, Beato M. Recurrent excitation between motoneurones propagates across segments and is purely glutamatergic. PLoS Biol. 2018;16: e2003586.

72. Danner SM, Zhang H, Shevtsova NA, Borowska J, Rybak IA, Zhang Y. Spinal V3 interneurons and left-right coordination in mammalian locomotion [Internet]. doi:10.1101/679654

73. Kiehn O. Decoding the organization of spinal circuits that control locomotion. Nat Rev Neurosci. 2016;17: 224–238.

74. Dougherty KJ, Zagoraiou L, Satoh D, Rozani I, Doobar S, Arber S, et al. Locomotor rhythm generation linked to the output of spinal shox2 excitatory interneurons. Neuron. 2013;80: 920–933.

75. Caldeira V, Dougherty KJ, Borgius L, Kiehn O. Spinal Hb9::Cre-derived excitatory interneurons contribute to rhythm generation in the mouse. Sci Rep. 2017;7: 41369.

76. Jean-Xavier C, Mentis GZ, O'Donovan MJ, Cattaert D, Vinay L. Dual personality of GABA/glycine-mediated depolarizations in immature spinal cord. Proc Natl Acad Sci U S A. 2007;104: 11477–11482.

77. Reimer MM, Norris A, Ohnmacht J, Patani R, Zhong Z, Dias TB, et al. Dopamine from the brain promotes spinal motor neuron generation during development and adult regeneration. Dev Cell. 2013;25: 478–491.

78. Lambert AM, Bonkowsky JL, Masino MA. The conserved dopaminergic diencephalospinal tract mediates vertebrate locomotor development in zebrafish larvae. J Neurosci. 2012;32: 13488–13500.

79. Pflieger J-F, Clarac F, Vinay L. Postural modifications and neuronal excitability changes induced by a short-term serotonin depletion during neonatal development in the rat. J Neurosci. 2002;22: 5108–

5117.

80. Gackiere F., Vinay L. Serotonergic modulation of post-synaptic inhibition and locomotor alternating pattern in the spinal cord. Front Neural Circuits. 2014;8. doi:10.3389/fncir.2014.00102

81. Whelan P, Bonnot A, O'Donovan MJ. Properties of rhythmic activity generated by the isolated spinal cord of the neonatal mouse. J Neurophysiol. 2000;84: 2821–2833.

82. Nakanishi ST, Whelan PJ. Diversification of intrinsic motoneuron electrical properties during normal development and botulinum toxin-induced muscle paralysis in early postnatal mice. J Neurophysiol. 2010;103: 2833–2845.

83. Mor Y, Lev-Tov A. Analysis of rhythmic patterns produced by spinal neural networks. J Neurophysiol. 2007;98: 2807–2817.

84. Han P, Nakanishi ST, Tran MA, Whelan PJ. Dopaminergic Modulation of Spinal Neuronal Excitability. Journal of Neuroscience. 2007;27: 13192–13204.